This is to certify that the

dissertation entitled

INFRARED LASER STARK LINE SHAPES: COLLISIONAL
NARROWING IN CH_3CN AND ZERO FIELD LEVEL
CROSSING IN $^{13}CH_3F$

presented by

Scott Thomas Sandholm

has been accepted towards fulfillment
of the requirements for

___Ph.D.___ degree in _Chemistry_

Major professor

R. H. Schwendeman

Date_June 18, 1982_

INFRARED LASER STARK LINE SHAPES: COLLISIONAL

NARROWING IN CH_3CN AND ZERO FIELD LEVEL CROSSING IN $^{13}CH_3F$

By

Scott Thomas Sandholm

A DISSERTATION

Submitted to
Michigan State University
in partial fulfillment of the requirements
for the degree of

DOCTOR OF PHILOSOPHY

Department of Chemistry

1982

ABSTRACT

INFRARED LASER STARK LINE SHAPES: COLLISIONAL
NARROWING IN CH_3CN AND ZERO FIELD LEVEL CROSSING IN $^{13}CH_3F$

By

Scott Thomas Sandholm

Two different infrared laser Stark line shape experiments were employed for investigation of collisional relaxation processes in molecular systems. The first experiment was a conventional linear absorption study of the line shape of the JKM = 211 ← 111 transition in the ν_4 vibration-rotation band of CH_3CN at fixed infrared frequency as a function of electric field. The second experiment was a study of zero field level crossing in the R(4,3) transition in the ν_3 band of $^{13}CH_3F$. The infrared laser Stark spectrometer used in these investigations and the necessary theories are described.

In order to obtain a satisfactory interpretation of the data in the investigation of the CH_3CN line shape, it was necessary to include the phenomenon of collisional narrowing. The conventional Voigt profile used to interpret combined collisional and Doppler

.

broadening was unable to explain all of the results obtained. However, either of the limiting hard collision or soft collision models of a Doppler broadened, Dicke narrowed, Lorentz broadened line shape yielded adequate explanations of the experimental results. For the soft collision model the pressure broadening parameter was 69.4 ± 0.7 MHz/torr and the narrowing parameter was 17.2 ± 1.7 MHz/torr. For the hard collision model the pressure broadening parameter was 11.5 ± 1.2 MHz/torr.

The non-linear level crossing effect in $^{13}CH_3F$ is a result of a near coincidence of the frequency of the transition with that of a CO_2 laser line. The line shape of the effect was studied as a function of electric field as the field passes through zero. For this Doppler-free effect the laser was stabilized against the fluorescence Lamb dip in CO_2. The experimental line shapes were fit to the sum of a Lorentz function and a polynomial background. Calculated line shapes, generated from a theory of zero-field level crossing, were also fit. By adjusting parameters in the theoretical calculations, good agreement between theory and experiment was obtained. The effective pressure broadening parameter for this transition was determined to be 16.0 ± 0.9 MHz/torr.

To Mom and Dad

ACKNOWLEDGMENT

TABLE OF CONTENTS

LIST OF TABLES

vii

LIST OF FIGURES

ix

CHAPTER I

WHY LINE SHAPE STUDIES?

There are many applications for the information obtained from line shape experiments. Gas laser and plasma discharge investigators find measurements of line shapes a useful analytic technique as do astronomers probing interstellar space. Line shape data include band parameters as well as kinetic relaxation information. Scientists also find line shape information useful in atmospheric and air pollution measurements.

Astronomers have used line shape measurements for the determination of molecular[1-14] abundance and relative isotopic abundance in outer space. Different isotopic species of a given molecule (carbon in CO, HCN, and H_2CO, oxygen in CO, H_2CO, and OH, nitrogen in HCN, and NH_3, sulfur in CS)[1] in different interstellar objects have been studied. Researchers have investigated the atmospheres of other planets by line shape studies. For example, hydrogen, methane, and ammonia on Jupiter,[3-7] carbon monoxide and carbon dioxide on Mars,[2] and carbon dioxide on Venus[2] have been analyzed. They have also used line shapes to probe interstellar gas clouds[8-14] and stars[11]

for thermodynamic structure, movement, and column density.

Line shape studies lead to band parameters, since spectroscopic constants are calculated from transition frequencies. A line shape study generates an insight into collisional phenomena, which is more relevant to this investigation. Line shape investigations of collisional relaxation can lead to a measure of the population relaxation time (denoted by $T_1^{(12)}$ and associated with the diagonal elements of the density matrix) or to the induced polarization relaxation time (denoted by $T_2^{(12)}$ and associated with the off-diagonal elements of the density matrix). These times, T_1 and T_2, are the optical analogs of the NMR relaxation times.

The collisions contributing to T_2-type relaxations can be categorized into three types: (1) collisions in which there is a change in energy; (2) collisions in which there is only a change in the M quantum number, and (3) collisions in which there is only a change in the phase of the molecular wavefunctions. Either transient or steady state measurements can be applied to investigate relaxation times. Multipulse transient-effect experiments[15-17] measure the population relaxation whereas the photon echo[16-18] and free induction decay[16-19] (also called optical nutation or coherent optical ringing) transient-effect experiments measure the induced polarization relaxation time. Steady state line width experiments can

be measurements of either linear absorption line shapes
or partially saturated line shapes. From linear absorption
studies only T_2 can be obtained, whereas both T_1 and T_2
can sometimes be obtained from studies of partially satu-
rated line shapes.

Accurate steady state line shape measurements in the
infrared are relatively new; grating monochrometers and
Fourier transform infrared (FTIR) spectrometers have not
had the necessary resolution (grating-type monochrometers
have ~ 0.1 cm^{-1} resolution whereas until recently FTIR
spectrometers were limited to ~ 0.05 cm^{-1} resolution). Re-
cently, infrared diode lasers have been used as a probe in
line shape experiments. One of the difficulties with tun-
able diode lasers is that frequency measurements are not as
simple or as reliable as with gas lasers. Also, the tun-
ability of diode lasers leaves a lot to be desired; during
scanning, the output frequency can be a step function or
not even a monotonic function of time. The small size
of the diode lasers creates the inherent problem of a
large divergence angle. The laser lines in gas lasers
have well known fixed frequencies and a Stark electric
field or microwave radiation field can be used to sweep
through a spectrum. The resolution of a laser Stark
spectrometer is much smaller than the Doppler width of
the transitions. Microwave two photon or double reson-
ance experiments with fixed frequency lasers have both

tunability and a highly accurate frequency scale. High power gas lasers, such as CO_2 and N_2O lasers, make it possible to obtain measurements of Doppler-free line widths of saturated spectra as well as of level crossings, avoided crossings, Lamb dips, or inverted Lamb dips.[17]

The application of line shape measurements to gas laser design[25] can be as simple as the use of the band parameters to indicate possible laseable lines to as complicated as the use of these parameters to optimize optical resonance transfer lasers (ORTL) systems. Typical ORTL systems involve a CO_2 laser pumping another gas and creating a far infrared laser. Examples of gases used for submillimeter CW lasers are CH_3F, $^{13}CH_3F$, and CH_3CN.[20-24] A molecular transition has to be pressure broadened to pump the system into a population inversion, but not pressure broadened excessively causing collisional de-excitation. A methyl fluoride laser pumped by a CO_2 laser has been built that is continually tunable between 150 μm and 1 mm.[24] The MIT group that designed and built this laser see a potential use in remote sensing applications, probably for measurements of atmospheric pollutants.

Molecular line shapes of CO_2,[2] SO_2,[27] N_2O,[28] and NO_2[27] have been studied because of their possible effects on the earth's environment. The partial pressure of carbon dioxide in the atmosphere is an important parameter in the green house effect, which concerns the

heat balance on earth. Also, sulfur and NO_x compounds can be monitored spectroscopically and their concentration determined, if air broadening information is available.

CHAPTER II

INTRODUCTION TO LASER STARK LINE SHAPES AND

COLLISIONAL NARROWING

This chapter is an overview of the determination of
the pressure broadening parameter for a vibration-rotation
transition in acetonitrile, CH_3CN. Acetonitrile has a
large dipole moment (3.93 D[29]) as well as a vibration-
rotation that is resonant with an N_2O laser line at a low
electric field, two important criteria for pressure de-
pendent infrared laser Stark experiments. A large pres-
sure broadening contribution to the line shape is expected
as a result of the large dipole moment and the fact that
pure rotational transitions have large pressure broadening
parameters.[30] For the transition selected, the $^QR_1(1)$
line in the ν_4 vibration-rotation band, sample pressures
above one torr are attainable before an electrical dis-
charge occurs in the sample cell, because the transition
is resonant with the P(20) N_2O laser line at a relatively
low electric field (1009 volts/cm).[31]

The conventional line shape for fitting pressure broad-
ened infrared spectral line shapes is known as a Voigt
profile,[32] a convolution of Lorentzian and Gaussian

6

line shapes. After deconvolution of the spectral data, the pressure broadening component is expected to be linear in pressure. Also, a slightly positive intercept at zero pressure is expected in the plot of pressure broadening vs. pressure. The intercept results from beam transit and wall broadening effects. The first laser Stark line shape data for the transition under consideration were taken by Dr. E. Bjarnov and analyzed by means of a Voigt profile. A bowed line in the low pressure region was obtained. Alternatively, an unsatisfactory negative intercept was obtained from a linear regression analysis of the high pressure points.[33] Many possible explanations for the discrepancy were investigated: addition of the second order Stark effect to the fitting, increasing the cell spacing to eliminate the effect of possible infrared reflections in the cell, laser power broadening, incorrect effective Doppler width, and dimerization of CH_3CN. None of these effects could explain the results. It was therefore concluded that the departure from linearity is real and that the Voigt line shape is an unsatisfactory representation of the experimental data.

Late in 1952 R. H. Dicke wrote a theoretical paper[34] on a line narrowing effect which has become known as collisional or Dicke narrowing. Dicke narrowing has been detected in HF[35] and HCl[36] by using a tunable difference frequency laser spectrometer, in H_2 and D_2 by

means of multipole techniques (CARS,[37,38] stimulated Raman gain,[39] high resolution Raman scattering,[40-42] and both quadrapole[43-45] and electric field[46] induced absorption), and H_2O[47] by using a diode infrared laser. This dissertation describes the first experimental evidence of collisional or Dicke narrowing in a laser Stark spectrum. Unlike the H_2O and HCl experiments, where Xe and/or Ar were used as foreign gas broadeners, this report will be on the self broadening of CH_3CN.

CHAPTER III

EXPERIMENTAL DETAILS OF THE CH_3CN

INVESTIGATION

3.1. Hardware

The laser spectrometer used in the present experiment
is virtually the same as that used in our laboratory for
the laser Stark spectroscopy of POF_3[48] (Figure 1). The
radiation source is a CO_2 or N_2O laser with a water-cooled
plasma tube and NaCl Brewster angle windows. The laser
cavity is mounted in an invar frame with a partially-trans-
mitting, dielectric-coated, germanium mirror at one end
and a 150 lines/mm plane grating blazed at 10 μm at the
other end. In these experiments the laser was stabilized
near the top of the laser gain profile and the day-to-day
frequency variation of the laser was approximately ±3 MHz.

The sample cell consists of a pair of nickel plates,
40 x 5 x 2 cm, with rounded edges and broad faces that
have been ground flat to within ±0.5 μm. The nickel plates
are separated by polished optically flat quartz spacers
(0.1 or 0.3 cm). To produce the desired electric field
the output from a D.C. power supply (Fluke Model 410B)
is connected to one plate and the output from a

9

Figure 1. A block diagram of the laser Stark spectrom-
            eter used in these experiments.

11
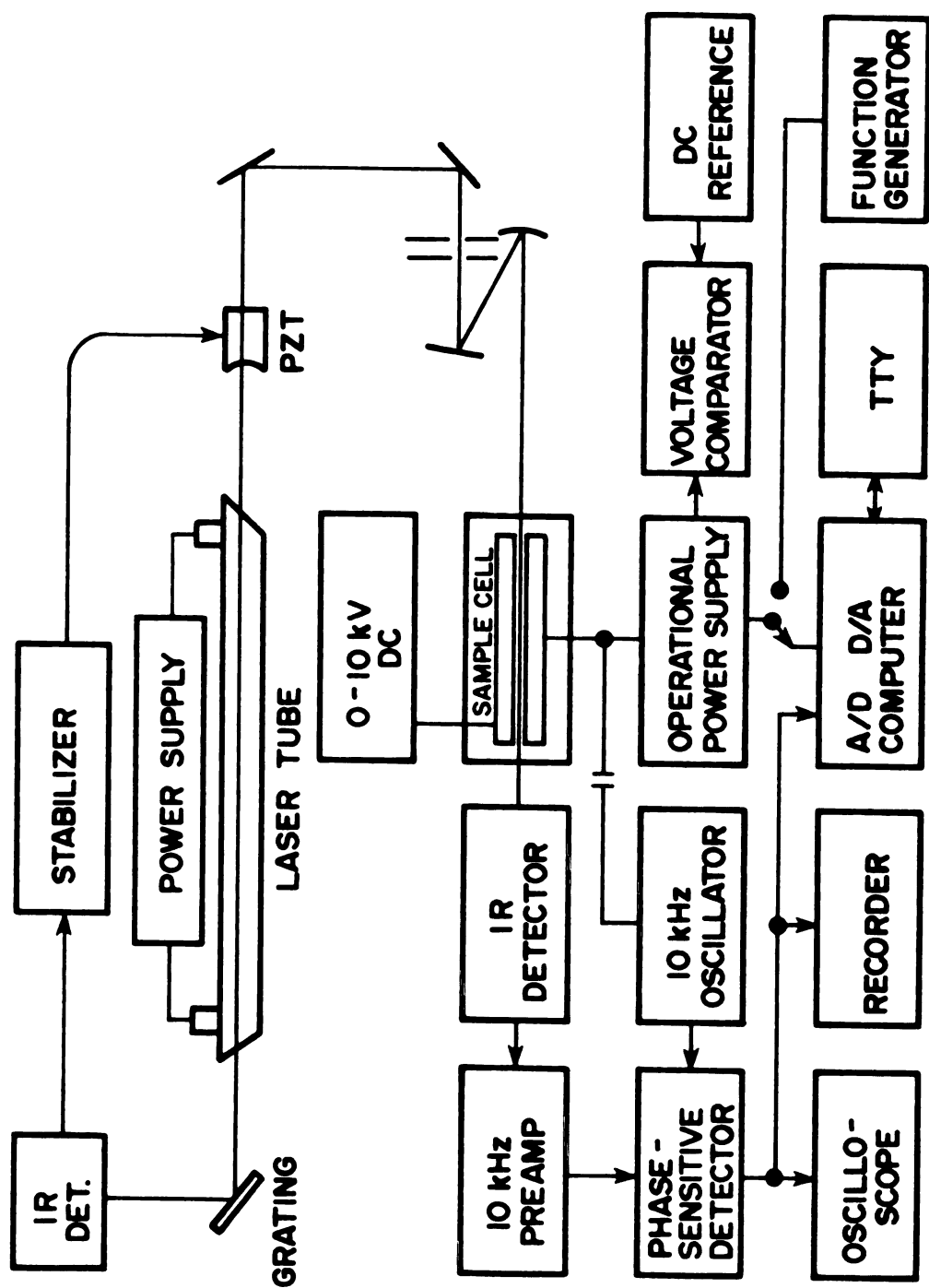
INFRARED LASER – STARK SPECTROMETER

Figure 1

computer-driven operational power supply (Kepco Model 2000)
is mixed with a 10 kHz sine wave voltage and connected to
the other plate. The sine wave voltage provides low-am-
plitude modulation of the Stark field. The separation
of the plates (0.29894 cm in the experiments described
here) was determined spectroscopically by measuring
the resonant voltage of the saturation dip in the
Q(1,1) transition in the ν_3 band of CH_3F; a 9P(32) CO_2
laser line was used. The resonant voltage was divided by
the resonant field reported by Frend et al.[49] to obtain
the cell spacing. Sample pressures are measured with two
different capacitance manometers (MKS Model 77 and Model
220B Baratrons); in the present experiments the pressure
ranged up to ∿1 torr. After passing through the cell the
laser radiation is monitored by a Pb-Sn-Te photovoltaic
detector (Barnes Engineering). The detector output is
processed by a phase-sensitive detector and is stored in
a Digital Equipment Corporation PDP-8E computer as well
as being displayed on an oscilloscope. The computer also
controls the voltage of the operational power supply.

3.2. The Sample of CH_3CN

The acetonitrile was obtained from Mr. Walter Cleland
at MSU who had purified a reagent grade sample by double
distillation,[50,51] first in CaH_2 to remove any water and
second in phosphorus pentoxide to remove the last traces

of water and any acidic impurities. As already mentioned, acetonitrile was chosen as an initial sample because the $(J,k,m) = (2,\pm 1,\pm 1) \leftarrow (1,\pm 1,\pm 1)$ transition in the ν_4 band resonates with the P(20) N_2O laser line at low electric field (1009.25 volts/cm).[31] This allows one to reach relatively high pressures without an electrical discharge in the sample cell.

3.3. Software

For this study, four major line shape fitting programs were used: a Voigt profile program and three programs essential to the Dicke narrowing aspects of this research. The two major contributors to the software development were Drs. E. Bjarnov and R. H. Schwendeman; Bjarnov for the Voigt fitting program VGTFIT and Schwendeman for the Dicke narrowing programs DNRFIT (for the soft collision model), DNHFIT (for the hard collision model), and DNGFIT (the Gaussian fitting program).

The hard collision model is appropriate when the velocity of the molecule under study after a collision is independent of its velocity before the collision,[53] and the soft collision model is proper when several collisions are required to produce a substantial change in the direction of travel. The DNGFIT program was used in the lower pressure region (below 50 millitorr) to determine an experimental Doppler width. In this program the

narrowing (Dicke) and the broadening (Lorentzian) parameters were held constant and the Doppler width allowed to vary.

All of the fitting programs read a data file and perform a least squares adjustment of several parameters to fit the data to the derivative of the appropriate theoretical equation. The derived fitting parameters are printed along with the standard errors, variance-covariance matrix, and correlation matrix. The derivative functions are a result of the experimental method used to obtain the data (phase sensitive detection of a small amplitude modulated signal). All of the calculations and fittings were performed in the MSU CYBER 750 computer.

Another program indispensable to the data acquisition in these experiments is BOXM. This program for the PDP8/E computer is virtually the same as the BOXA program used in earlier laser Stark experiments from this laboratory.[52] The new name is a result of changes required to implement a new computer interface designed and built by Mr. Martin Rabb at MSU. The BOXM program increments a digital to analog converter that controls the operational power supply attached to one plate in the sample cell. After each increment in electric field, the program delays for a predetermined period of time and then reads the spectrometer output by means of an analog to digital converter (A/D). The A/D is read an optional number of times with a preselected

time period between readings. The field sweep may be repeated a selected number of times and all of the A/D readings at each field setting are averaged. The stored data are continuously displayed on an oscilloscope during acquisition. After acquisition, the stored data may be filed on a flexible disc for permanent storage and later data treatment.

CHAPTER IV

THEORY

There is a wealth of information hidden in spectral line shapes or profiles. The amplitude of absorption as a function of frequency can lead to information about the concentration of a sample as well as to the transition frequency. More relevant to this research are the pressure broadening parameters, which are useful in the design of optical resonant transfer lasers, as well as for measurements of chemical abundance in the atmosphere or outer space or for the determination of motion in the interstellar media. Also, information pertaining to relaxation processes and collision dynamics in the molecular system is obtained from line shape investigations. In order to determine this kind of information from spectral lines, an understanding of what gives rise to the various line shapes is required.

If a molecule could be represented by a stationary "free particle", its spectra would have a natural line width from spontaneous emission and uncertainty broadening (a result of the Heisenberg uncertainty principle). If the "free particle" is allowed to interact with its

surrounding through collisions, but yet frozen in space
(everything is allowed to have translational motion ex-
cept for the molecule undergoing the transition), the
width of the line would grow. Collisional or pressure
broadening may take place by several mechanisms - self or
resonant broadening (collisions with like molecules),
foreign gas broadening (collisions with unlike molecules),
or wall broadening (collisions with the sample cell or
container walls). All of the processes mentioned so far
result in homogeneously broadened line shapes, because each
molecule is allowed to absorb radiation over the entire
line profile. The exponential decay of the dipole cor-
relation for these collision relaxation processes result
in Lorentzian line shapes.

If the "free particle" is allowed to have transla-
tional motion, the Doppler effect, beam transit effects,
and Dicke or collisional narrowing can contribute to the
spectral line shape. The Doppler effect can be traced
back to 1842 when Christian Doppler of Prague first noted
a velocity dependent frequency shift. Velocity shifts are
a very important part of infrared line shapes in gaseous
samples. Dicke or collisional narrowing is the result of
the molecule experiencing multiple collisions before travel-
ing a distance of $\lambda/2\pi$.[53] If the narrowing mechanism
is not taken into consideration when interpreting the
results some experiments show a reduced effective Doppler

width. The beam transit effects result from excited or
hot molecules moving out of the beam and being replaced
in the beam by ground state or cold molecules, a pseudo
relaxation process. Beam transit effects and wall broaden-
ing are calculated by the kinetic theory of gases, after
assuming that the resulting line shape is the same as that
due to intermolecular collisions.

Modulation broadening, another potential contributor
to line broadening, occurs when the experimental modula-
tion amplitude is too large. Recall that the small ampli-
tude modulation is the reason for the derivative line
shapes. A derivative of a function F is defined by,

$$F'(x) \equiv \lim_{h \to o} \frac{F(x+h)-F(x)}{h} \quad . \qquad (1)$$

Then, the modulation amplitude being too large is analog-
ous to the derivative not being evaluated in the limit as
$h \to o$.

If one could freeze the gas molecules in place to
eliminate any translational motion (i.e., remove the Doppler
contribution to the line shape), the spectral line from a
laser Stark experiment would fit a Lorentzian equation.
Then the steady state absorption coefficient at low radia-
tion power would be

$$\gamma_L(\omega_L) = \frac{\gamma_o \, \Delta\omega_L^2}{(\omega_\ell - \omega_o)^2 + \Delta\omega_L^2} \quad , \tag{2}$$

which can be shown to result from the steady state solution of the optical Bloch equations.[12,54,55] The peak absorption coefficient γ_o occurs at $\omega_\ell = \omega_o$ and is defined by

$$\gamma_o = \frac{4\pi\omega_o\mu_{if}^2\Delta N_o}{h \, c \, \Delta\omega_L} \quad , \tag{3}$$

where the initial population difference between the two levels is ΔN_o and μ_{if} is the transition dipole moment matrix element,

$$\mu_{if} = \langle J'k'm'|\mu_F|J''k''m''\rangle \quad . \tag{4}$$

Here μ_F is the molecular dipole moment along the space fixed axis F[56] in the direction of the applied radiation electric vector. The half width at half height for absorption by the molecule at a single velocity is $\Delta\omega_L$. This is represented by,

$$\Delta\omega_L = (2\pi T_2)^{-1} \quad , \tag{5}$$

where T_2 is the relaxation time for the induced electric field polarization.

If the molecules are allowed to have translational motion, they will move randomly in all directions with an isotropic velocity distribution (i.e., a Maxwell-Boltzmann distribution).[57] The Doppler motion will contribute to the line shape in such a way that the profile will no longer be Lorentzian. If the Doppler and pressure broadening mechanisms are independent, and if the Lorentzian profile is folded into the Gaussian distribution of the Doppler broadened line, a new line shape is generated. This convoluted line shape, first studied by Voigt[32] in 1912, fails to give a simple analytic result for the integrated absorption coefficient; it can, however, be written as an integral, as follows

$$\gamma = \left(\frac{M}{2\pi k_B T}\right)^{1/2} \frac{\gamma_0 \, c \, \Delta\omega_L^2}{\omega_\ell} \int_{-\infty}^{\infty} \frac{\exp\left[\frac{-M}{2k_B T}\left(\frac{c\omega_s}{\omega_\ell}\right)^2\right]}{(\omega_\ell - \omega_0 - \omega_s)^2 + \Delta\omega_L^2} \, d\omega_s \; .$$

(6)

In this expression, in addition to the quantities already defined, M is the molecular mass of the absorbing molecule, k_B is the Boltzmann constant, T is the absolute temperature, and ω_s is the Doppler shift in frequency ($\omega_s = \omega_\ell(v/c)$ where v is the component of the velocity of the molecule in the direction of the radiation).

A study of the low pressure line shape of CH_3F vibration-rotation transitions showed that in the low pressure

limit ($\Delta\omega_D \gg \Delta\omega_L$) the expected limiting Gaussian shape of the Voigt equation is obtained experimentally.[52] At intermediate pressures and under certain circumstances, the spectral line shape can be deconvoluted into its Guassian and Lorentzian components. From the Lorentzian moiety, it can be shown that the half width at half maximum should be linear in pressure with a slightly positive intercept. The intercept is not expected to be situated at the origin because of the beam transit and wall broadening relaxation processes. The slope of this line would be the pressure broadening parameter for the particular transition and the molecular system. The parameter would be a self broadening or a foreign gas broadening parameter, or a mixture of the two, depending on the nature of the collision partners.

The Voigt equation used in this investigation is a derivative of Equation (6) with respect to the electric field,

$$S(\varepsilon) = \frac{2A \, \Delta\omega_L}{\pi^{3/2}\sigma} \left(\frac{\partial x}{\partial \varepsilon}\right)_0 \int_{-\infty}^{\infty} \frac{(x+y)\exp(-y^2/\sigma^2)}{[(x+y)^2 + \Delta\omega_L^2]^2} \, dy +$$

$$+ B(\varepsilon-\varepsilon_0) + C \quad , \tag{7}$$

where

$$x = \omega_\ell - \omega_o = \left(\frac{\partial \omega_o}{\partial \varepsilon}\right)_o (\varepsilon - \varepsilon_o) + \frac{1}{2} \left(\frac{\partial^2 \omega_o^2}{\partial \varepsilon^2}\right) (\varepsilon - \varepsilon_o)^2 \quad , \quad (8)$$

and

$$\sigma = \left(\frac{2k_BT}{M}\right)^{1/2} \frac{\omega_\ell}{c} = \Delta\omega_D/(\ell n2)^{1/2} \quad . \quad (9)$$

The constant σ is referred to as the reduced Doppler width; $\Delta\omega_D$ is the ordinary Doppler half width at half maximum. Five parameters are fit in a least squares calculation: the amplitude (A), the center field (ε_o), the Lorentz width ($\Delta\omega_L$), a slope (B), and a background (C). The spectrometer scans through the electric field ε, which is measured in volts per centimeter. The derivatives $(\partial\omega_o/\partial\varepsilon)_o$ and $(\partial^2\omega_o/\partial\varepsilon^2)_o$ are obtained from the known spectroscopic parameters and dipole moments of the sample.

In 1952, R. H. Dicke published an article[34] on what has come to be called Dicke or collisional narrowing. Quantum mechanically the Doppler effect is treated as a recoil momentum transferred from the photon to the absorber molecule,[58] a Mössbauer effect in gases. If the pressure is such that the collision time is short in comparison to the time between collisions, then the momentum can be absorbed by a single molecule. This is the case where one would expect a Voigt profile to fit the spectral data satisfactorily. If the molecule experiences several velocity changing collisions before the molecular dipole

undergoes a single cycle while following the radiation, then the effective Doppler shift is an average of the shifts produced by the velocities between the collisions. If the wavelength divided by 2π is comparable to the mean free path between collisions, the spectral line is expected to be narrowed. In other words, the molecule experiences several collisions before traveling a wavelength.

Since Dicke's original work, the theory has been expanded and modified by Galatry[59] and by Rautian and Sobel'man[53] among others[60,61] and there have been several models devised to deal with this phenomenon. Two limiting models have been considered in this investigation: the "soft" or "weak" collision model and the "hard" or "strong" collision model.

In the soft collision model the spectral line shape has been shown to be[35,39]

$$I_{sc}(\omega) = (I_o/\pi) \int_o^\infty \exp[-\Delta\omega_L\tau - (\sigma^2/\beta_{sc}^2)$$

$$x \; \{\exp(-\beta_{sc}\tau)-1-\beta_{sc}\tau\}]\cos[(\omega_\ell-\omega_o)\tau]d\tau \; . \qquad (10)$$

After substitution from Equation (8) and differentiation with respect to electric field, an expression for the spectrometer signal is obtained as follows:

$$S(\varepsilon) = \frac{-A}{\pi} \left(\frac{\partial x}{\partial \varepsilon}\right)_0 \int_0^\infty \tau \exp[-y(\tau)]\sin(x\tau)d\tau + B(\varepsilon-\varepsilon_0) + C.$$

(11)

In these expressions,

$$y(\tau) = -\Delta\omega_L\tau - \frac{\sigma^2}{2\beta_{sc}^2}[\exp(-\beta_{sc}\tau)-1-\beta_{sc}\tau] \quad ,$$

(12)

β_{sc} is the narrowing parameter,[53,59] and A, B, C, x, σ, and $\Delta\omega_L$ have the same definitions as in the Voigt equation.

In the hard collision model the line shape function is,[35,53,59,61]

$$I_{hc}(\omega) = (I_0/\pi) \text{ Re}[F/(1-\beta_{hc}F)] \quad ,$$

(13)

where

$$F = (\pi^{1/2}\sigma)^{-1} \int_{-\infty}^\infty \frac{\exp(-\tau^2/\sigma^2)}{[\beta_{hc}+\Delta\omega_L+i(\tau-x)]}d\tau \quad ,$$

(14)

so that the spectrometer signal is,

$$S(\varepsilon) = \frac{A}{\pi} \text{ Re } \left[\frac{Q}{(1-\beta_{hc}F)^2}\right] + \beta_{hc}(\varepsilon-\varepsilon_0) + C \quad .$$

(15)

and

$$Q = \left(\frac{\partial F}{\partial \varepsilon}\right)_0 = \frac{-i}{\pi^{1/2}\sigma} \left(\frac{\partial x}{\partial \varepsilon}\right)_0 \int_{-\infty}^\infty \frac{\exp(-\tau^2/\sigma^2)}{[\Delta\omega_L+\beta_{hc}+i(\tau-x)]} \quad .$$

(16)

Again, the previous definitions of A, B, C, $\Delta\omega_L$, x, and

σ hold, and β_{hc} is the hard collision model narrowing

parameter. A classic example of a hard collision in

foreign gas broadening is the kind in which a small light

molecule is being observed while colliding with a large

heavy molecule; for a soft collision the situation is

just the reverse.

To close this section on the line broadening processes,

it is appropriate to present a quantitative explanation

of the wall broadening and beam transit effects, since

they are used to help determine the intercepts in the de-

termination of both the pressure broadening parameter and

the narrowing parameter. The beam transit effect can

be considered a subset of the wall broadening relaxation

processes, only with beam transit relaxation the walls

are not solid objects, but rather the imaginary boundary of

the laser beam. Then, if the line shape for the wall col-

lisions is assumed to be the same as for intermolecular

collisions (not a bad assumption since both processes

involve collisional de-excitation), a line broadening

parameter similar to Equation (5) can be assumed, where the

relaxation time is the mean free time from the kinetic

theory of gases. The wall broadening relaxation parameter

then is,[62]

$$\Delta\omega_{wb} = \frac{A}{V} \left(\frac{RT}{8\pi^3 M}\right)^{1/2} \quad , \tag{17}$$

where R is the gas constant, T is the absolute temperature, M is the molecular mass, V is the irradiated volume, and A is the surface area surrounding the irradiated volume.

CHAPTER V

RESULTS AND CONCLUSIONS

5.1. Treatment of the Raw Data

All of the data were temperature corrected to 298 K
(the data were collected at room temperature). A short
explanation of the method employed for the correction is
given in this section. The derived half width at half
height $\Delta\omega_L$ is a function of the temperature (T), the
narrowing parameter (β), and the Doppler width $\Delta\omega_D$. There-
fore,

$$\frac{d\Delta\omega_L}{dT} = \left(\frac{\partial\delta\omega_L}{\partial T}\right) + \left(\frac{\partial\Delta\omega_L}{\partial\beta}\right)\left(\frac{\partial\beta}{\partial T}\right) + \left(\frac{\partial\Delta\omega_L}{\partial\Delta\omega_D}\right)\left(\frac{\partial\Delta\omega_D}{\partial T}\right) \quad . \tag{18}$$

Also,

$$\Delta\omega_L(298K) = \Delta\omega_L(T_{Exp.}) + \left(\frac{d\Delta\omega_L}{dT}\right) dT \quad . \tag{19}$$

If $dT \approx \Delta T = 298 - T_{Exp.}$, $\tag{20}$

then

$$\Delta\omega_L(298K) = \Delta\omega_L (T_{Exp.}) + (\frac{d\Delta\omega_L}{dT}) (298-T_{Exp.}), \quad (21)$$

so that

$$\Delta\omega_L(298K) = \Delta\omega_L(T_{Exp.}) + \{ (\frac{\partial\Delta\omega_L}{\partial T}) + (\frac{\partial\Delta\omega_L}{\partial\beta})(\frac{\partial\beta}{\partial T}) +$$

$$+ (\frac{\partial\Delta\omega_L}{\partial\Delta\omega_D})(\frac{\partial\Delta\omega_D}{\partial T})\} (298-T_{Exp.}) \quad . \quad (22)$$

From Equation (9),

$$\Delta\omega_D = \omega_\ell (\frac{T}{M})^{1/2} (3.5815 \times 10^{-7}) \quad . \quad (23)$$

To obtain expressions for $(\partial\beta/\partial T)$ and $(\partial\Delta\omega_L/\partial T)$ it was assumed that

$$\beta = k_\beta/T \quad , \quad (24)$$

and

$$\Delta\omega_L = k_L/T \quad . \quad (25)$$

Then,

$$\Delta\omega_L(298K) = \Delta\omega_L(T_{Exp.}) + (\frac{298-T_{Exp.}}{298})\{ (\frac{\partial\Delta\omega_L}{\partial\Delta\omega_D})(\frac{\Delta\omega_D}{2})$$

$$- (\frac{\partial\Delta\omega_L}{\partial\beta})\beta - \Delta\omega_L (T_{Exp.})\} \quad . \quad (26)$$

The iterative manner in which β is calculated generates a wealth of data on the functional relationship between β and $\Delta\omega_L$ from which the $(\partial\Delta\omega_L/\partial\beta)$ can be determined. The derivative $(\partial\Delta\omega_L/\partial\Delta\omega_D)$ required calculations of the pressure broadening parameter for slightly different Doppler widths. A linear interpolation of the data generated a satisfactory value for the derivative. All of the temperature corrected data are listed in Table (I).

5.2. Experimental Determination of the Doppler Width

At very low pressure there is not a significant number of collisions to cause much pressure broadening and at high pressures there is much more pressure broadening than in homogeneous broadening. It then follows that a better estimate of the pressure broadening can be obtained from the data taken at higher pressure, and a better measurement of the Doppler width can be obtained from the low pressure data.

The experimental Doppler width was determined by first using the theoretical Doppler width with the data above 300 millitorr to determine the pressure broadening and Dicke narrowing parameters. Then, the pressure broadening parameter was held constant and the low pressure data (below 50 millitorr) were used to derive the Doppler width parameter. The experimental Doppler width was used and held constant in the fit of all of the data to determine a

Table I.   Acetonitrile Laser Stark Pressure Broadened Half
            Width at Half Maximum for the Soft Collision,
            Hard Collision and Voigt Profile Models (T=298K).

Pressure mtorr[a]	$\Delta\nu_L$/MHz (soft)[b,c]	$\Delta\nu_L$/MHz (Hard)[b,d]	$\Delta\nu_L$/MHz (Voigt)[b,e]
1299.	90.55±0.73	89.90±0.75	87.78±0.82
1194.	82.81±0.46	82.19±0.47	79.95±0.49
973.56	67.09±0.33	66.37±0.28	63.82±0.22
945.60	65.40±0.13	64.81±0.12	62.26±0.06
918.36	63.34±0.17	62.25±0.16	60.10±0.05
878.21	60.89±0.20	60.23±0.20	57.73±0.28
845.37	57.81±0.40	57.19±0.40	54.72±0.42
839.79	58.23±0.38	57.54±0.34	55.11±0.36
805.18	56.26±0.05	55.62±0.05	53.15±0.06
801.37	55.16±0.27	54.50±0.28	52.09±0.30
770.25	53.65±0.12	53.01±0.12	50.54±0.13
720.07	49.81±0.09	49.22±0.10	46.66±0.12
674.10	46.94±0.11	46.31±0.11	43.79±0.17
617.48	43.21±0.20	42.52±0.21	40.15±0.20
565.69	39.05±0.13	38.55±0.13	35.97±0.13
564.37	39.26±0.07	38.72±0.07	36.21±0.09
542.11	38.07±0.16	37.51±0.16	35.02±0.16
514.16	35.88±0.10	35.36±0.11	32.88±0.10
500.30	34.89±0.15	34.44±0.14	31.78±0.14
496.38	34.74±0.35	34.24±0.35	31.86±0.50
484.65	33.92±0.15	33.40±0.15	30.80±0.15
460.37	32.38±0.29	32.00±0.29	29.39±0.29
454.71	31.36±0.08	30.92±0.09	28.45±0.09
438.64	30.56±0.21	30.00±0.21	27.44±0.26
420.03	29.00±0.14	29.75±0.14	36.12±0.15
419.78	29.29±0.19	28.85±0.19	26.29±0.21
398.45	27.80±0.24	27.42±0.24	24.83±0.25
383.87	26.62±0.06	26.30±0.06	23.74±0.07
377.84	26.47±0.15	26.09±0.15	23.57±0.16
357.99	24.87±0.19	24.53±0.18	22.03±0.21
353.44	24.33±0.07	24.05±0.07	21.53±0.07
331.39	23.23±0.10	23.01±0.10	20.54±0.10
128.24	9.15±0.14	9.19±0.13	7.56±0.15
109.50	7.53±0.10	7.56±0.09	6.16±0.10
97.79	6.49±0.10	6.55±0.10	5.20±0.12
93.68	6.32±0.11	6.43±0.11	5.10±0.11
87.18	5.64±0.11	5.55±0.11	4.62±0.08
76.31	5.28±0.13	5.41±0.12	4.37±0.13
72.89	4.88±0.09	5.01±0.09	4.03±0.09

Table I. Continued.

[a]Pressure measured with a Baratron capacitance monometer (MKS type 77 or type 2203).

[b]The error limits are the standard errors from the least square fits.

[c]Temperature-corrected data obtained from fits of Equation (11). In the numerical integration by Simpson's rule, 40 points were included with $\Delta\tau=0.006$ μs.

[d]Temperature-corrected data obtained from fits to Equation (15). In the numerical integration by Simpson's rule, 40 points were included with $\Delta\tau=2.5$ MHz.

[e]Temperature-corrected data obtained from fits to equation (7). In the numerical integration by Simpson's rule 40 points were included with $\Delta y=2.5$ MHz.

pressure broadening and collisional narrowing parameter

(Table II). It was assumed that any effect of modulation

Table II. Line Shape Parameters.

CH_3CN: $(J,K,M) = (2,\pm 1,\pm 1) \leftarrow (1,\pm 1,\pm 1)$
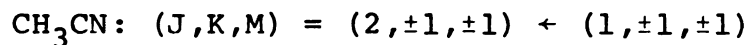
Model	$\Delta \nu_L$	β
Soft Collision	69.4±0.7 MHz/torr	17.2±2 MHz/torr
Hard Collision	68.6±0.7 MHz/torr	11.5±2 MHz/torr

broadening would be taken into account by using the experi-

mental Doppler width. Theoretical calculations of the

effect of modulation broadening on the value of the pres-

sure broadening parameter obtained, where the modulation

amplitude was approximately that used in the experiments,

proved this to be the case. The theoretical Doppler width

at 298K is 26.7 MHz, whereas the experimental Doppler width

was found to be 27.0 ± 0.26 MHz (±2σ).

5.3. Determination of the Narrowing Parameter

It was stated earlier that the beam transit and wall

broadening effects were used in the determination of the

narrowing parameter. But, in order to calculate the wall

broadening, the irradiated volume, as well as the

33

corresponding surface area, had to be determined. It was assumed that the geometry of the volume was that of a cylinder whose height was equal to the length of the Stark plates (40 cm) and whose diameter was approximately equal to the cell spacing (0.3 cm). The radius of the cylinder is based on the fact that the laser beam was collimated with two iris diaphragms with 3 mm openings. The wall broadening parameter obtained by using the kinetic theory of gas model is on the order of 15 kHz at 298K. The narrowing parameter (β) was varied by interpolation or extrapolation until a straight line with a reasonable intercept, was obtained for the plot of $\Delta\omega_L$ vs. pressure.

5.4. Final Results

The temperature-corrected data for the models used in this investigation are listed in Table (I). A graph of the pressure broadening vs. pressure based on the soft collision model and on the Voigt profile are shown in Figure 2. The slope of the plot, the collisional broadening parameter for the soft collision model, is 69.4±0.7 MHz/torr; the intercept is 21±94 kHz. The slope of the plot of the Voigt profile data is 67.7±0.7 MHz/torr with an intercept of -1.77±0.17 MHz.

The temperature-corrected $\Delta\omega_L$'s for the hard collision model and the Voigt profile are represented in

Figure 2. Plot of the pressure broadening <u>vs</u> pressure
for the JKM = 211←111 transition in the ν_4
band of CH_3CN; soft collision model assumed.
Solid line is the best straight line through
the circles; slope = 69.4 MHz/torr, intercept
= 0.021 MHz.
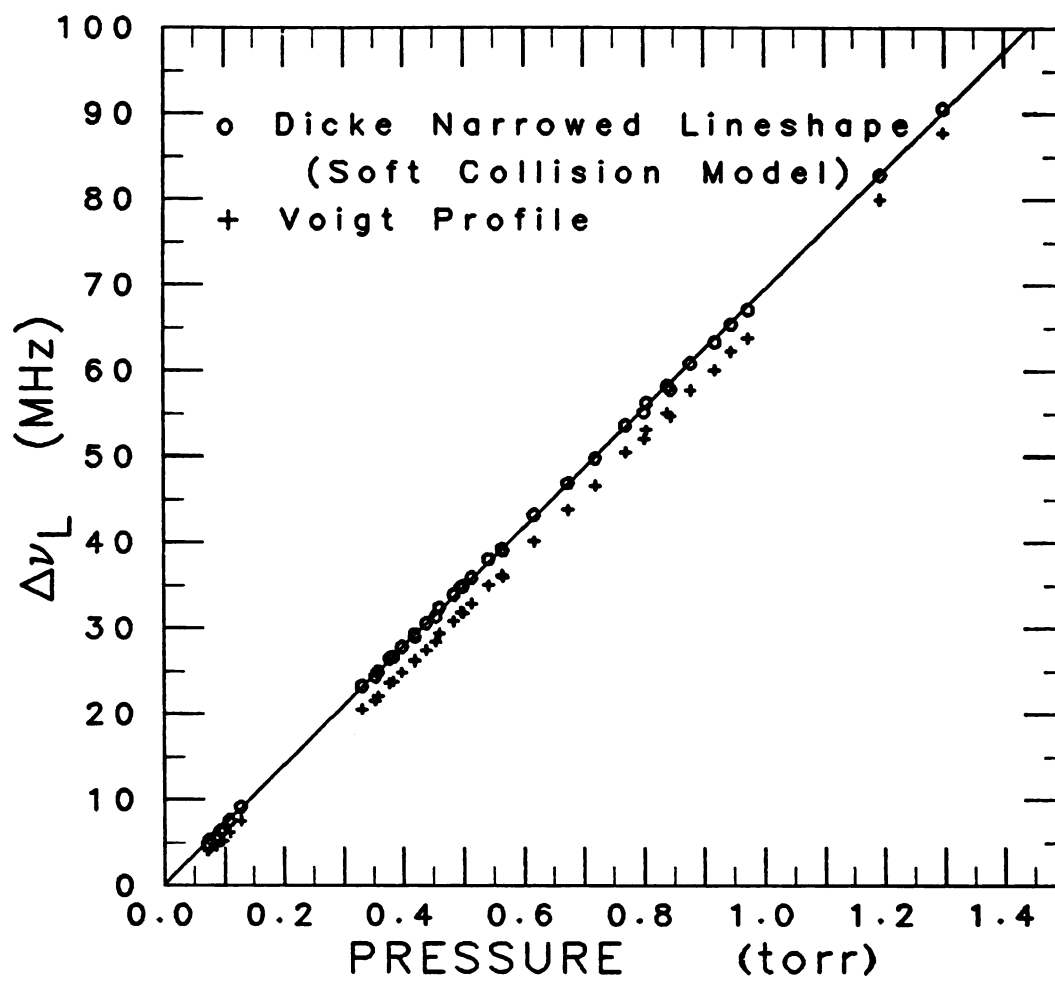
Figure 2

graphical form by Figure 3. The collisional broadening parameter for the hard collision model is 68.6±0.7 MHz/ torr with an intercept of 25±90 kHz.

The large standard errors in the intercept in each case reflect back into uncertainty in determination of the narrowing parameter. The Dicke narrowing parameter for the soft collision model is 17.2±1.7 MHz/torr, while that for the hard collision model is 11.5±1.2 MHz/torr. The uncertainties given above for the intercepts is one standard error, as calculated from the linear regression analysis. The errors given for the slopes are mainly the result of an estimated 1% error in the pressure measurement. The error limits for the narrowing parameters were handled in a much more subjective manner. The value reported is 10% of the narrowing parameter and was based on a judgment of the sensitivity of the determined value of β to the uncertainty in the intercept. It was noted during the course of the determination of the narrowing parameter that a very small change in β creates a rather large change in the intercept.

Inclusion of the collisional narrowing in the fitting of the observed laser Stark line shape has produced two positive results: First, the plot of pressure broadening vs. pressure is now a straight line with a reasonable intercept. Second, a value of the collisional narrowing parameter can be estimated. This does not solve all of

Figure 3. Plot of the pressure broadening $\underline{vs}$ pressure
for the JKM = 211←111 transition in the ν_4
band of CH_3CN; hard collision model assumed.
Solid line is the best straight line through
the circles; slope = 68.6 MHz/torr, intercept
= 0.025 MHz.
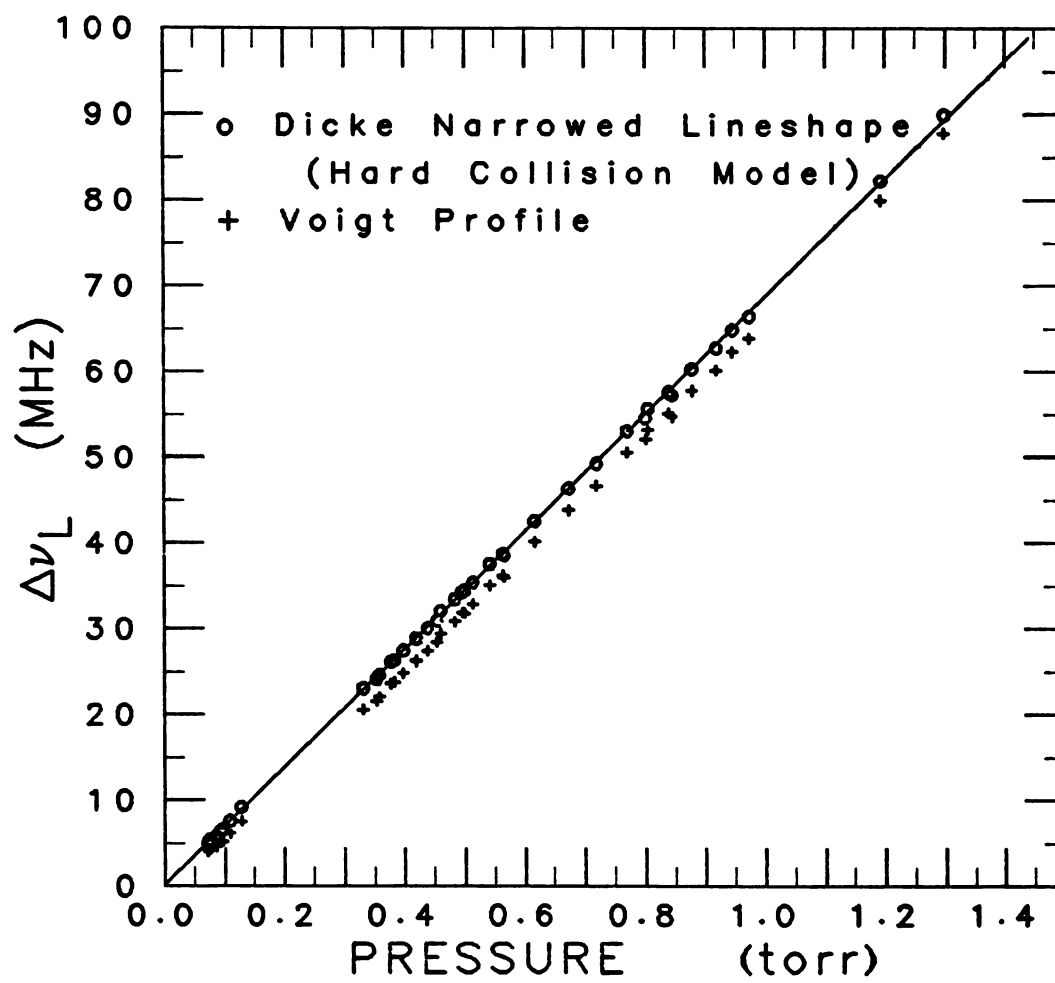
Figure 3

the problems, but rather creates a small dilemma: the data fit the hard collision model just as well as the soft collision model, and so do not allow a choice to be made between them.

It would not be appropriate to close without commenting on two other possible explanations considered for the curvature in the Voigt line: power broadening and dimerization. Power broadening is a possible explanation for the curvature, but corrections for power broadening would lead to a line with an even more negative intercept. Concerning the dimerization a calculation based on an estimated value of the dimerization constant[63] indicates that there would be less than 0.1% dimer in the sample cell at one torr pressure. The effect of this small amount of dimer is at least an order of magnitude less than the effect of the error in the pressure measurement.

The narrowing parameter (β) has been interpreted as the reciprocal of the mean time between velocity-changing collisions. If it is assumed that every kinetic theory collision is hard enough to cause a change in direction, then the kinetic theory collision diameter can provide an estimate of the lower limit to β. Based on the Stockmayer potential, the acetonitrile collision diameter has been estimated to be ≈ 4 Å,[63] which leads to $\beta_{k.t.} = 1.4$ MHz/torr. The kinetic theory narrowing parameter ($\beta_{k.t.}$) is approximately ten times smaller than the determined values.

CHAPTER VI

INTRODUCTION TO LEVEL CROSSING AND ANTICROSSING

Level crossing is a more general form of the Hanle effect[64] depolarization of fluorescence radiation in a magnetic field), which dates back to 1924. In 1959, Colegrove and co-workers[65] carried out the first application of level crossing to fine structure determination, in a study of the effect of magnetic field on fluorescence from He. Since then, many molecules have been studied both by level crossing experiments (Xe,[66] H_2,[67] CH_4,[68-70] CH_3F[71,72] and CD_3I[74]) and avoided crossing experiments (CD_3I,[74] Li,[75] POF_3,[76,77] and the CN radical[78]). A variety of experimental techniques and spectral regions have been used for both level crossing and anticrossing measurements: Zeeman fluorescence,[67,75] Zeeman effect on absorption,[69] Stark effects on infrared laser[68,74,76] and microwave[72] spectroscopy, and radio frequency induced crossings.[70,71]

The theory of level crossing and avoided crossing has been considered by a number of authors;[75,76,78,79] most were concerned with the effect on detection of fluorescence, rather than on detection of absorption. In the

study of the effect of level crossing or anticrossing on fluorescence induced by weak radiation, saturation effects may be ignored. By contrast, level crossing or anticrossing is a non-linear effect in direct absorption and therefore saturation effects are crucial. Shimoda[79] presented a theory of the effect of level crossing on a single mode laser field; Sakai and Katayama[74] developed perturbation theories for the effect of crossing and anticrossing on direct absorption; and Amano and Schwendeman[76] extended the earlier theories to a higher order of approximation. An extension of the theory of Amano and Schwendeman was used in this investigation.

Level crossing or anticrossing occurs when two levels become degenerate as a result of the shifting of the molecular energy levels by an electric or magnetic field. Both terms refer to saturation phenomena and which effect occurs depends on whether the crossing levels are connected by a non-zero matrix element of the Hamiltonian for the system. Consider a three level system in which the two levels that become degenerate are lower in energy than the third level (Figure 4). If the matrix element connecting the two levels that cross is zero, and the transition dipole moments connecting the crossing levels to the third level are nonzero, a level crossing is expected. If the matrix element between the two levels that cross is non-zero and one of the transition dipole moments connecting

Figure 4. A diagram of a simple three level crossing
crossing and level anticrossing.
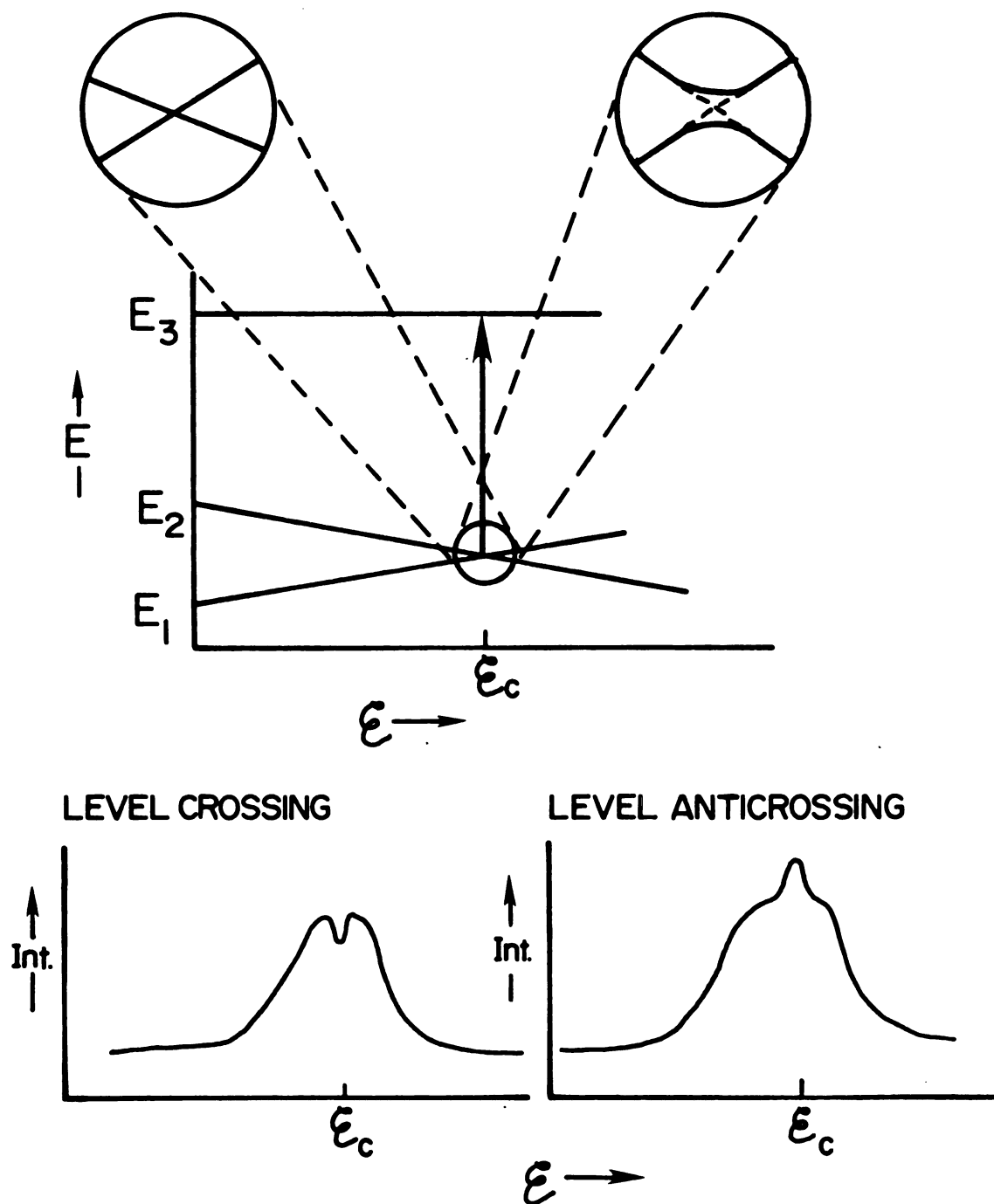
Figure 4

the crossing levels to the third level is non-zero, a level anticrossing or Von Neuman avoided crossing is expected.

The term level crossing is almost self explanatory in terms of the effect on the molecular energy levels. As the two levels become degenerate in the Stark field, there is no interaction between the two levels because the matrix element between them is zero. The wave functions do not mix and the energy levels cross. The anticrossing or avoided crossing term is a little more ambiguous. The matrix element between the two levels that cross is non-zero in the avoided crossing; therefore, as the levels proceed toward degeneracy, a mixing of the states occurs and the crossing is prevented by the interaction between the two levels.

In the simple case of a level crossing in an infrared laser Stark experiment the laser pumps molecules out of the lower two levels, sampling from different velocity groups. As the Stark field is swept through the level crossing, the velocity groups corresponding to the transitions change. At the electric field corresponding to the crossing, both transitions are pumping out of the same molecular velocity group and the effect of the additional saturation can be detected as a dip in the absorption. In the case of an avoided crossing in infrared laser Stark spectroscopy only one of the lower state to upper state transitions is allowed when the field is far from the value at which the

levels would cross, if they could.   As the Stark field is
swept through the crossing region, a mixing of the anti-
crossing wavefunction occurs.   At the electric field of
closest approach for the avoided crossing there is a
maximum in the intensity borrowing.   Because the two tran-
sitions sample different velocity groups, saturation is
reduced and there is an increase in the signal strength.

CHAPTER VII

EXPERIMENTAL DETAILS OF THE $^{13}CH_3F$ ZERO FIELD LEVEL CROSSING

7.1. The Spectrometer

The laser Stark spectrometer is virtually the same as that used in the Dicke narrowing experiments (Figure 1) and only the modifications necessary to do the zero field level crossing will be discussed. In all of the other laser Stark experiments the electric field was swept from some positive lower dc value to a higher positive dc value. In the zero field level crossing experiment it is essential that the electric field be swept through zero field. To accomplish this the polarity of the output of the power supply (Fluke 410B) applied to one plate in the sample cell was reversed so that its voltage opposed that of the output of the operational power supply applied to the other plate. The Stark electric field voltage ranged from ±5 to ±20 volts depending on the width of the level crossing effect.

7.2. Stabilization

The previous laser Stark experiments used a dither stabilization method in which the piezoelectric transla- tor (PZT), which supports the partially transmitting mirror, was modulated at 520 Hz. The resulting modulation of the length of the laser cavity was used to lock the laser fre- quency to the value at the top of the laser gain profile (through phase sensitive detection).

For the zero field level crossing experiments the laser was locked to the minimum of a saturation dip (Lamb dip) in the fluorescence from a CO_2 gas sample. A detector (Judson model J10D InSb) was mounted over a BaF_2 window in the side of a brass tube for the detection of the CO_2 fluorescence.

The tube, with ZnSe Brewster angle windows, was placed within the laser cavity. The inside of the tube was polished to enhance the fluorescence reaching the detector. The laser was frequency modulated by application of a sine wave voltage to the PZT. A derivative lineshape of the fluorescence signal was produced by a phase sensitive detector and used with a feedback loop to the PZT to con- trol the frequency of the laser. This method of frequency stabilization was tested and compared to the dither laser gain method by repeated measurements of a CH_3F laser Stark Lamp dip; the results are reported in a later section.

7.3. Laser Power Measurements

Because the zero field level crossing signal is a saturation phenomenon, it is necessary to properly measure the laser power in order to account for the power broadening in the detected signal. A laser power meter (Scientech Incorporated Model 36001) was used to monitor the laser output. The laser power entering the Stark cell was measured at the beginning and at the end of each day at a point approximately 75 cm from the mirror used to partially focus the laser radiation into the sample cell. During the day, the laser power reflected from a beam splitter was continuously monitored. It was assumed that if the laser power, as measured off the beam splitter, did not fluctuate, the power was also constant in the Stark cell. The laser power measured before the Stark cell ranged from 17 mW to 37 mW from day to day, but only varied ±2.5 mW within a day.

7.4. Computer Programs

As in the other laser Stark experiments, the BOXM program was used for data acquisition. Typical input parameters were as follows: 200 channels with 3 sweeps; integration number (number of A/D converter readings at each field) from 10 to 30, depending on the signal strength; timing number (time between readings of the A/D converter

at each field) either 5, 10 or 20 centiseconds, always chosen to be at least 3 times as large as the time constant on the lock-in amplifier; delay number (additional time before the first A/D converter reading at each field) 5 or 10 centiseconds.

A program called LDFIT3 was used for fitting the spectral data. This is a PDP-8 program which fits the background to a polynomial and the level crossing to a derivative of a Lorentzian line shape. The amplitude, halfwidth at half maximum, and center electric field of the Lorentzian as well as the coefficients of linear and cubic terms in the polynomial were varied in the fitting. A program LDFIT2, which fit the signal to a Gaussian derivative was found to be a poorer way to fit the background than the polynomial. A program LDFIT, which fits the background to a linear equation with a slope and intercept failed miserably for the zero field level crossing.

Modulation broadening effects were investigated theoretically by generating modulation-broadened zero field level crossing signals on the PDP-8. These curves, which were based on the polynomial plus a Lorentzian line shape, were fit with the LDFIT3 program.

Theoretical line shapes were generated exactly by using the program LVX2 on the CYBER 750 computer, and fit to the polynomial minus a Lorentzian. The input required for the program LVX2 includes the Stark slopes

for all the different m states, the laser electric field amplitude, and a pressure broadening parameter. By varying the laser electric field factor and the pressure broadening parameter, data corresponding to the experimental line shapes were generated.

7.5. The Sample

The sample of carbon 13 fluoromethane was obtained from Merck and Company, Incorporated. The sample had 90 atom % isotopic carbon 13 and was used as received.

CHAPTER VIII

THEORY

8.1. <u>Solution of the Density Matrix Equation of Motion</u>

The lineshape theory of the level crossing effect begins
with the density matrix equation of motion[12,80]

$$ih\dot{\rho} = [H_T, \rho] \quad , \tag{27}$$

where the total Hamiltonian H_T is,

$$H_T = H^O + H^R + H^C \tag{28}$$

and

$$H^R = - \mu \cdot \underset{\sim}{\varepsilon}_R \quad . \tag{29}$$

In Equation (28), H^R is the contribution to the Hamiltonian
from the radiation, H^C represents the collisional relaxa-
tion terms, and H^O is the molecular Hamiltonian in a static
Stark electric field ε. In the three level system dis-
cussed earlier the crossing levels are labeled 1 and 2,
and the upper level is labeled 3. The crossing Stark

field is denoted by ε_C and the corresponding transition

energy by $\hbar\omega_C$. Then by the previous explanation of cross-

ing and avoided crossing, $H_{12} = 0$ or $H_{12} \neq 0$, respectively.

The elements for the density matrix equation of motion,

in a basis in which $H_{12} = 0$, are

$$\dot{\rho}_{11} = \frac{-i}{\hbar}[H^R_{13}\rho_{31} - \rho_{13}H^R_{31}] - \gamma_{11}(\rho_{11} - \rho^O_{11}) \ , \tag{30}$$

$$\dot{\rho}_{22} = \frac{-i}{\hbar}[H^R_{23}\rho_{32} - \rho_{23}H^R_{32}] - \gamma_{22}(\rho_{22} - \rho^O_{22}) \ , \tag{31}$$

$$\dot{\rho}_{33} = \frac{-i}{\hbar}[H^R_{31}\rho_{13} + H^R_{32}\rho_{23} - \rho_{31}H^R_{13} - \rho_{32}H^R_{23}] - \gamma_{33}(\rho_{33} - \rho^O_{33})$$
$$\tag{32}$$

$$\dot{\rho}_{21} = \frac{-i}{\hbar}[H^R_{23}\rho_{31} - \rho_{23}H^R_{31} + H^O_{22}\rho_{21} - \rho_{21}H^O_{11}] - \gamma_{21}\rho_{21} \ , \tag{33}$$

$$\dot{\rho}_{31} = \frac{-i}{\hbar}[H^R_{31}\rho_{11} + H^R_{32}\rho_{21} + H^O_{33}\rho_{31} - \rho_{32}H^O_{11} - \rho_{33}H^R_{31}] - \gamma_{32}\rho_{32} \ ,$$
$$\tag{34}$$

$$\dot{\rho}_{32} = \frac{-i}{\hbar}[H^R_{31}\rho_{12} + H^R_{32}\rho_{22} + H^O_{33}\rho_{32} - \rho_{32}H^O_{22} - \rho_{33}H^R_{32}] - \gamma_{32}\rho_{32} \ .$$
$$\tag{35}$$

The phenomenological relaxation times γ_{11}, γ_{22}, γ_{33}, γ_{21},

γ_{31}, and γ_{32} have been introduced to represent the col-

lisional relaxation effects of H^C. The applied laser

radiator is assumed to be of the form,

$$\varepsilon_R = \varepsilon_\ell \cos(\omega_\ell t - kz) \ , \tag{36}$$

then

$$H_{fi}^{R} = -\mu_{fi}\varepsilon_{\ell}\cos(\omega_{\ell}t-kz). \tag{37}$$

If

$$\omega_{fi} = (H_{ff}^{O}-H_{ii}^{O})/h \; , \tag{38}$$

$$\mu_{13} = \mu_{31} \neq 0 \; , \tag{39}$$

and

$$\mu_{23} = \mu_{32} \neq 0 \; , \tag{40}$$

then the density matrix elements become

$$\dot{\rho}_{11} = \frac{i\varepsilon_{\ell}}{h}[\mu_{31}(\rho_{31}-\rho_{13})]\cos\omega_{\ell}t - \gamma_{11}(\rho_{11}-\rho_{11}^{O}) \; , \tag{41}$$

$$\dot{\rho}_{22} = \frac{i\varepsilon_{\ell}}{h}[\mu_{32}(\rho_{32}-\rho_{23})]\cos\omega_{\ell}t - \gamma_{22}(\rho_{22}-\rho_{22}^{O}) \; , \tag{42}$$

$$\dot{\rho}_{33} = \frac{-i\varepsilon_{\ell}}{h}[\mu_{31}(\rho_{31}-\rho_{13})+\mu_{23}(\rho_{32}-\rho_{23})]\cos\omega_{\ell}t$$

$$- \gamma_{33}(\rho_{33}-\rho_{33}^{O}) \; , \tag{43}$$

$$\dot{\rho}_{21} = -i\omega_{21}\rho_{21} + \frac{i\varepsilon_{\ell}}{h}[\mu_{32}\rho_{31} - \mu_{31}\rho_{23}]\cos\omega_{\ell}t - \gamma_{21}\rho_{21} \; ,$$

$$\tag{44}$$

$$\dot{\rho}_{31} = -i\omega_{31}\rho_{31} + \frac{i\varepsilon_\ell}{\hbar}[\mu_{31}(\rho_{11}-\rho_{33}) + \mu_{32}\rho_{21}]\cos\omega_\ell t$$

$$- \gamma_{31}\rho_{31} , \tag{45}$$

$$\dot{\rho}_{32} = -i\omega_{32}\rho_{32} + \frac{i\varepsilon_\ell}{\hbar}[\mu_{31}\rho_{12} + \mu_{32}(\rho_{22}-\rho_{33})]\cos\omega_\ell t$$

$$- \gamma_{32}\rho_{32} . \tag{46}$$

If

$$X_{fi} = \varepsilon_\ell\mu_{fi}/\hbar , \tag{47}$$

then X_{fi} represents a power broadening term in the line shape. The laser radiation excites the 3←1 and the 3←2 transitions, and the off-diagonal density matrix elements will follow the radiation field as

$$\rho_{31} = \bar{\rho}_{31}\exp -i(\omega_\ell t-kz) , \tag{48}$$

$$\rho_{32} = \bar{\rho}_{32}\exp -i(\omega_\ell t-kz) . \tag{49}$$

Here the preexponentials are the peak values of the ρ_{fi} terms. Note that to a good approximation the density matrix element for the 2←1 transition does not follow the radiation field and therefore is not an explicit function of the laser frequency.

After the rotating wave approximation (the dipole moments cannot follow the high frequency terms), the density matrix elements become

$$\dot{\rho}_{11} = \frac{iX_{31}}{2}(\bar{\rho}_{31}-\bar{\rho}_{13}) - \gamma_{11}(\rho_{11}-\rho_{11}^{o}) \ , \tag{50}$$

$$\dot{\rho}_{22} = \frac{iX_{32}}{2}(\bar{\rho}_{32}-\bar{\rho}_{23}) - \gamma_{22}(\rho_{22}-\rho_{22}^{o}) \ , \tag{51}$$

$$\dot{\rho}_{33} = \frac{-iX_{31}}{2}(\bar{\rho}_{31}-\bar{\rho}_{13}) + \frac{iX_{32}}{2}(\bar{\rho}_{23}-\bar{\rho}_{32}) - \gamma_{33}(\rho_{33}-\rho_{33}^{o}) \ , \tag{52}$$

$$\dot{\rho}_{21} = -i\omega_{21}\rho_{21} + \frac{iX_{32}}{2}\bar{\rho}_{31} - \frac{iX_{31}}{2}\bar{\rho}_{23} - \gamma_{21}\rho_{21} \ , \tag{53}$$

$$\dot{\rho}_{31}e^{-i\omega t} - i\omega\bar{\rho}_{31}e^{-i\omega t} = -i\omega_{31}\bar{\rho}_{31}e^{-i\omega t} + \frac{iX_{31}}{2}(\rho_{11}-\rho_{33})e^{-i\omega t}$$

$$+ \frac{iX_{32}}{2}\rho_{21}e^{-i\omega t} - \gamma_{31}\bar{\rho}_{31}e^{-i\omega t} \ , \tag{54}$$

$$\dot{\rho}_{32}e^{-i\omega t} - i\omega\bar{\rho}_{32}e^{-i\omega t} = -i\omega_{32}\bar{\rho}_{32}e^{-i\omega t} + \frac{iX_{31}}{2}\rho_{21}e^{-i\omega t}$$

$$+ \frac{iX_{32}}{2}(\rho_{22}-\rho_{33})e^{-i\omega t} - \gamma_{32}\bar{\rho}_{32}e^{-i\omega t} \ . \tag{55}$$

Then, it follows that

$$\dot{\bar{\rho}}_{31} = i(\omega-\omega_{31})\bar{\rho}_{31} + \frac{iX_{31}}{2}(\rho_{11}-\rho_{33}) + \frac{iX_{32}}{2}\rho_{21} - \gamma_{31}\bar{\rho}_{31} \ , \tag{56}$$

$$\dot{\bar{\rho}}_{32} = i(\omega-\omega_{32})\bar{\rho}_{32} + \frac{iX_{32}}{2}(\rho_{22}-\rho_{33}) + \frac{iX_{31}}{2}\rho_{21} - \gamma_{32}\bar{\rho}_{32} \;.$$

(57)

Now, the density matrix elements are separated into pure imaginary and pure real components by letting

$$\rho_a = \rho_{11} - \rho_{33} \;,$$

(58)

$$\rho_b = \rho_{22} - \rho_{33} \;,$$

(59)

$$\Delta\rho_i = \rho_{ii} - \rho_{ii}^{o} \;,$$

(60)

$$\delta_{31} = \omega - \omega_{31} \;,$$

(61)

$$\delta_{32} = \omega - \omega_{32} \;,$$

(62)

$$\rho_{fi} = \rho_{fi}' + i\rho_{fi}'' \;,$$

(63)

and recalling that

$$\rho_{fi} = \rho_{if}^{*} \;.$$

(64)

Then, it follows that

$$\dot{\rho}_a = \dot{\rho}_{11} - \dot{\rho}_{33} = -2X_{31}\bar{\rho}_{31}'' - \gamma_{11}\Delta\rho_1 - X_{32}\bar{\rho}_{32}'' + \gamma_{33}\Delta\rho_3 \;,$$

(65)

$$\dot{\rho}_b = \dot{\rho}_{22} - \dot{\rho}_{33} = -2X_{32}\bar{\rho}''_{32} - \gamma_{22}\Delta\rho_2 - X_{31}\bar{\rho}''_{31} + \gamma_{33}\Delta\rho_3 \ ,$$

$$(66)$$

$$\dot{\rho}_{21} = -i\omega_{21}(\rho'_{21}+i\rho''_{21}) + \frac{iX_{32}}{2}(\bar{\rho}'_{31}+i\bar{\rho}''_{31}) - \frac{-iX_{31}}{2}(\bar{\rho}'_{32}-i\bar{\rho}''_{32}),$$

$$(67)$$

$$\dot{\bar{\rho}}_{31} = i\delta_{31}(\bar{\rho}'_{31}+i\bar{\rho}''_{31}) + \frac{iX_{31}}{2}\rho_a + iX_{32}(\rho'_{21}+i\rho''_{21})$$

$$- \gamma_{31}(\bar{\rho}'_{31}+i\bar{\rho}''_{31}) \ , \qquad (68)$$

$$\dot{\bar{\rho}}_{32} = i\delta_{32}(\bar{\rho}'_{32}+i\bar{\rho}''_{32}) + \frac{iX_{32}}{2}\rho_b + \frac{iX_{13}}{2}(\rho'_{21}-i\rho''_{21})$$

$$- \gamma_{32}(\bar{\rho}'_{32}+i\bar{\rho}''_{32}) \ . \qquad (69)$$

Clearly,

$$\dot{\rho}'_{21} = \omega_{21}\rho''_{21} - \frac{X_{32}}{2}\bar{\rho}''_{31} - \frac{X_{31}}{2}\bar{\rho}''_{32} - \gamma_{21}\rho'_{21} \ , \qquad (70)$$

$$\dot{\rho}''_{21} = -\omega_{21}\rho'_{21} + \frac{X_{32}}{2}\bar{\rho}'_{31} - \frac{X_{31}}{2}\bar{\rho}'_{32} - \gamma_{21}\rho''_{21} \ , \qquad (71)$$

$$\dot{\bar{\rho}}'_{31} = -\delta_{31}\bar{\rho}''_{31} - \frac{X_{23}}{2}\bar{\rho}''_{21} - \gamma_{31}\bar{\rho}'_{31} \ , \qquad (72)$$

$$\dot{\bar{\rho}}''_{31} = \delta_{31}\bar{\rho}'_{31} + \frac{X_{31}}{2}\rho_a + \frac{X_{32}}{2}\rho'_{21} - \gamma_{31}\bar{\rho}''_{31} \ , \qquad (73)$$

$$\dot{\bar{\rho}}'_{32} = -\delta_{32}\bar{\rho}''_{32} + \frac{X_{31}}{2}\rho''_{21} - \gamma_{32}\bar{\rho}'_{32} \ , \qquad (74)$$

$$\dot{\bar{\rho}}''_{32} = \delta_{32}\bar{\rho}'_{32} + \frac{X_{32}}{2}\rho_b + \frac{X_{31}}{2}\rho'_{21} - \gamma_{32}\bar{\rho}''_{32} \ . \qquad (75)$$

Next, ρ_a and ρ_b may be rewritten as

$$\rho_a = -2X_{31}\bar{\rho}''_{31} - X_{32}\bar{\rho}''_{32} - \frac{(\gamma_{11}-\gamma_{33})}{2}(\Delta\rho_1+\Delta\rho_3)$$

$$- \frac{(\gamma_{11}+\gamma_{33})}{2}(\Delta\rho_1-\Delta\rho_3) \quad , \tag{76}$$

and

$$\rho_b = -2X_{32}\bar{\rho}''_{32} - X_{31}\bar{\rho}''_{31} - \frac{(\gamma_{22}-\gamma_{33})}{2}(\Delta\rho_2+\Delta\rho_3)$$

$$- \frac{(\gamma_{22}+\gamma_{33})}{2}(\Delta\rho_2-\Delta\rho_3) \quad . \tag{77}$$

But $\gamma_{ii}-\gamma_{ff} \approx 0$ and $\Delta\rho_i+\Delta\rho_f \approx 0$ so that the product of these two terms is very small. Then, it is convenient to let

$$(\gamma_{11} + \gamma_{33})/2 = \gamma_a \tag{78}$$

which represents the collisional relaxation of the population difference of levels one and three, and to let

$$(\gamma_{22} + \gamma_{33})/2 = \gamma_b \tag{79}$$

which correspondingly represents the relaxation of the population difference of levels two and three.

Finally, the density matrix equation may be written in matrix form as

$$\dot{\underset{\sim}{L}} = -\underset{\sim}{A} \; \underset{\sim}{L} \; + \underset{\sim}{C} \tag{80}$$

where the transposes of $\underset{\sim}{L}$ and $\underset{\sim}{C}$ are

$$\underset{\sim}{L}^T = (\rho_a \quad \bar{\rho}'_{31} \quad \bar{\rho}''_{31} \quad \rho'_{21} \quad \rho''_{21} \quad \rho_b \quad \bar{\rho}'_{32} \quad \bar{\rho}''_{32}) \; , \tag{81}$$

and

$$\underset{\sim}{C}^T = (\gamma_a \rho_a^O \quad 0 \quad 0 \quad 0 \quad 0 \quad \gamma_b \rho_b^O \quad 0 \quad 0) \; , \tag{82}$$

and the $\underset{\sim}{A}$ matrix is

$$
\begin{pmatrix}
\gamma_a & 0 & 2X_{31} & 0 & 0 & 0 & 0 & X_{32} \\
0 & \gamma_{31} & \delta_{31} & 0 & X_{32}/2 & 0 & 0 & 0 \\
-X_{31}/2 & -\delta_{31} & \gamma_{31} & -X_{32}/2 & 0 & 0 & 0 & 0 \\
0 & 0 & X_{32}/2 & \gamma_{21} & -\omega_{21} & 0 & 0 & X_{31}/2 \\
0 & -X_{32}/2 & 0 & \omega_{21} & \gamma_{21} & 0 & X_{13}/2 & 0 \\
0 & X_{31} & 0 & 0 & 0 & \gamma_b & 0 & 2X_{32} \\
0 & 0 & 0 & 0 & -X_{31}/2 & 0 & \gamma_{32} & \delta_{32} \\
0 & 0 & 0 & -X_{31}/2 & 0 & -X_{32}/2 & -\delta_{32} & \gamma_{32}
\end{pmatrix}
$$

$$\tag{83}$$

The steady state solution to Equation (80) is

$$\underset{\sim}{L} = \underset{\sim}{A}^{-1} \underset{\sim}{C} , \qquad (84)$$

and the following is an outline of a method for solving this linear system.

(A) First use rows 4 and 5 to solve for ρ_{21}' and ρ_{21}'' and substitute back into the matrix. This reduces the 8 x 8 matrix to a 6 x 6 matrix.

(B) Use rows 1 and 4 of this reduced system to solve for ρ_a and ρ_b. After substitution, the system is reduced to a 4 x 4 matrix.

(C) The new 4 x 4 matrix can be reduced to a 2 x 2 matrix by solving for the real parts of $\bar{\rho}_{31}$ and $\bar{\rho}_{32}$.

(D) Solve the 2 x 2 system for $\bar{\rho}''_{31}$ and $\bar{\rho}''_{32}$.

The Doppler effect is an important contribution in infrared lineshape investigations; it quite often is the major contributor to the breadth of a laser Stark transition. The density matrix elements are Doppler averaged as follows

$$<\rho_{fi}> = \int_{-\infty}^{\infty} W(v) \rho_{fi} dv \qquad (85)$$

where

$$W(v) = \exp(-v^2/u^2)/\pi^{\frac{1}{2}}u \, , \tag{86}$$

with

$$u^2 = 2k_BT/M \, . \tag{87}$$

In these equations, v is the velocity of the molecule in the direction of the radiation, T is the absolute temperature, M is the molecular mass, and k_B is the Boltzmann constant. In this investigation the calculation of the Doppler averaged density matrix elements was carried out by numerical integration in a frequency vector space rather than a velocity coordinate system. The Doppler frequency shift is

$$\omega_s = \omega_{\rho\ell}v/c \, . \tag{88}$$

Therefore,

$$dv = (c/\omega_\ell) \, d\omega_s \tag{89}$$

and the Doppler averaging is

$$<\rho_{fi}> = \int_{-\infty}^{\infty} W(\omega_s)\rho_{fi} \, d\omega_s \tag{90}$$

where

$$W(\omega_s) = \exp(-\omega_s^2/\sigma^2)/\sqrt{\pi}\sigma \qquad (91)$$

with

$$\sigma = \Delta\nu_D/\sqrt{\ell n2} = u\omega_\ell/c ; \qquad (92)$$

$\Delta\nu_D$ is the usual Doppler half-width at half-height.

8.2. Absorption Coefficient

The polarization (P) can be written as the sum of an in-phase (with respect to the laser radiation) component (P_C) and an in-quadrature component (P_S),

$$P = P_C \cos(\omega_\ell t-kz) - P_S \sin(\omega_\ell t-kz) . \qquad (93)$$

The absorption coefficient (α) is proportional to the in-quadrature component of the polarization,

$$\alpha = -(4\pi\omega/c)(P_S/\varepsilon_\ell) , \qquad (94)$$

The polarization for an N particle gas with mean dipole moment $\langle\mu\rangle$ is denoted as

$$P = N\langle\mu\rangle . \qquad (95)$$

Then, since

$$\langle\mu\rangle = \text{tr}(\hat{\mu}\hat{\rho}) \, , \tag{96}$$

$$P = N\text{tr}(\hat{\mu} \, \hat{\rho}) \, , \tag{97}$$

and it follows that for the three level system defined previously, the polarization is

$$P = N[\mu_{13}(\langle\rho_{13}\rangle + \langle\rho_{31}\rangle) + \mu_{23}(\langle\rho_{23}\rangle + \langle\rho_{32}\rangle)]_o \tag{98}$$

Recall that the density matrix elements are related by

$$\rho_{31} = (\bar{\rho}'_{31} + i\bar{\rho}''_{31})e^{-i\omega t} \tag{99}$$

and

$$\rho_{13} = \rho_{31}^* = (\bar{\rho}'_{31} - i\bar{\rho}''_{31})e^{i\omega t} \, . \tag{100}$$

Therefore, the in-quadrature component of the polarization is

$$P_s = 2N[\mu_{13}\bar{\rho}''_{31} + \mu_{23}\bar{\rho}''_{32}] \, , \tag{101}$$

and the absorption coefficient is

$$\alpha = -(8\pi\omega N/c\varepsilon_\ell) \, (\mu_{13}\langle\bar{\rho}''_{31}\rangle + \mu_{23}\langle\bar{\rho}''_{32}\rangle) \, . \tag{102}$$

In the solution to the linear system $\bar{\rho}_{32}''$ and $\bar{\rho}_{31}'$ are solved for. After velocity averaging to obtain $<\bar{\rho}_{32}''>$ and $<\bar{\rho}_{31}''>$, these can be substituted into the absorption coefficient equation to give the lineshape for the simple level crossing system.

8.3. Multi Overlapping Level Crossings

In the zero field level crossing studied in this investigation there are more than just three levels involved and the energy relationship between the crossing pair and the third level differs for differing sets of levels. But, the biggest problem is what to do with states that are multiply pumped (i.e., states that are simultaneously involved in more than one level crossing). As a particular example consider the case in Figures 5 and 6. Note that each of the states in the lower level is the third level for a crossing pair in the upper level and also one member of a crossing pair with the third state in the upper level. Clearly, the problem is not as simple as the theory developed so far might have indicated. And, if the laser radiation pumps off-resonance, still another parameter must be considered.

The following assumptions were made in order to make the theory more tractable. First, since there is no way to separate the individual relaxation parameters, they are all treated as being equal; more eloquently stated,

Figure 5. A diagram of the multilevel zero field level crossing for the $^{13}CH_3F$ R(4,3) transition.
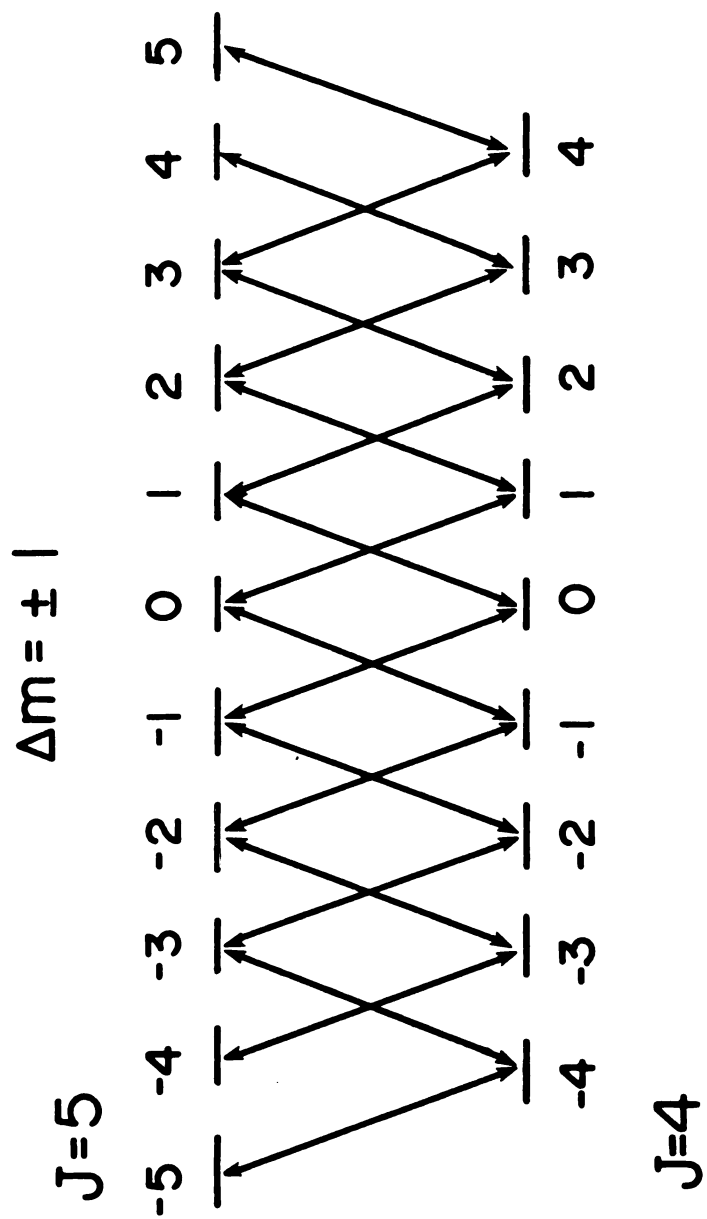
Figure 5

Figure 6. A diagram of the multilevel $^{13}CH_3F$ R(4,3) level crossing in the Stark electric field.

ZERO-FIELD LEVEL CROSSING (J=5 ← 4)

$\Delta m = \pm 1$

$\Delta k = 0$

$\Delta J = + 1$
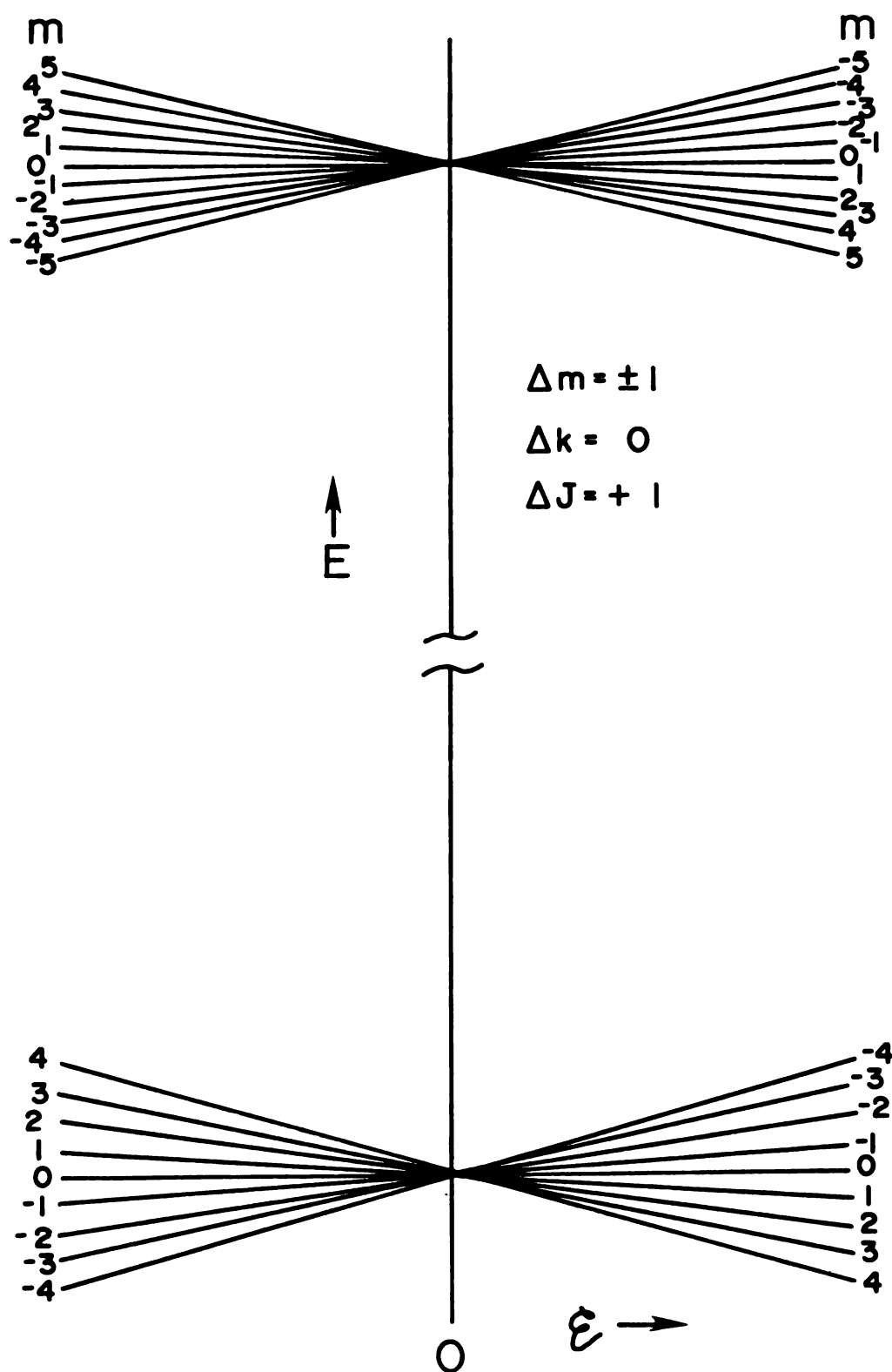
Figure 6

an effective relaxation parameter is measured. The problem of a state subjected to multiple pumping is handled in a more mundane fashion; the total crossing effect is treated as a sum of separate three-level systems. The last problem then is the off-resonance pumping. The difficulty arises not in the generation of the theoretical lineshapes but in the analysis of the measured line shapes. The off-resonance generates a background line shape that is the sum of all of the transitions. Each transition is off-resonance in the radiation electric field by a different amount, depending on the Stark slopes. Thus, some effort was required to determine a suitable form for the background on which the level crossing is superimposed.

8.4. Optics

8.4.a. Introduction

It is necessary to know the laser electric field amplitude (ε_ℓ) in order to calculate the power broadening factor (X_{fi}). In order to calculate the laser electric field emplitude inside the Stark cell it is necessary to know the beam waist, the divergence of the laser beam, the focal length as well as the location of all the mirrors and optics, and the size of the openings in any diaphragms and their locations. A measure of the laser power and the knowledge of the laser mode, with a TEM_{00} mode preferable,

are also required. The physical dimensions of the laser
determine the beam waist and the terminal optics of the
laser determine the spot size on the output mirror and
the beam divergence.

8.4.b. The Beam Waist, Divergence, and Focal Lengths

The geometry of the electric field distribution,
$\varepsilon_\ell (x,y)$, of the TEM_{00} mode of a transverse laser beam is
approximately described by the Gaussian expression,[80]

$$\varepsilon_\ell (x,y) = \varepsilon_o \exp \left(- \frac{x^2+y^2}{w^2}\right) , \tag{103}$$

or

$$\varepsilon_\ell (r) = \varepsilon_o \exp \left(-\frac{r^2}{w^2}\right) . \tag{104}$$

Here, w is the beam waist, or spot size radius, and can be
thought of as a measure of the standard deviation of the
amplitude of the laser beam. The beam waist at the sur-
face of the partially transmitting mirror at one end of the
laser cavity is given by[80,81]

$$w^4 = (\lambda R/\pi)^2/[(R/d) - 1], \tag{105}$$

when one mirror is flat and the other concave. The assump-
tion here is that the grating on the laser can be represented

approximately as a flat mirror. The spot size then is a function of the radius of the curved mirror (R), the spacing between the mirrors (d), and the wavelength (λ) of the radiation.

The laser beam will diverge as it leaves the laser cavity and the spot size can be calculated at some distance z from the output mirror as follows:

$$w_z = w[1 + \frac{z(f-R)}{Rf}] \tag{106}$$

where the focal length (f) is related to the index of refraction (n) of the material that the mirror is made of by

$$f = R/(n-1) . \tag{107}$$

Then, it can be shown that

$$w_z = w[1 + z(2-n)/R] . \tag{108}$$

The size of the diaphragms in the laser spectrometer (Figure 1) can be adjusted to limit the laser power going into the Stark cell. The radius of the laser beam (s) going into the Stark cell will be given by a similar equation as that of the spot size at some distance from the partially transmitting mirror, because the laser beam

will be diverging from the same source. Therefore,

$$s_z = s_d[1 + z(2-n)/R] , \qquad (109)$$

where s_d is the size of the opening in a diaphragm and s_z is the laser beam radius at some distance z from the diaphragm.

The mirror that focuses the laser beam into the Stark cell is a concave mirror with a four meter radius of curvature. Once the beam strikes this mirror it no longer diverges at the rate determined by the output mirror, but instead converges according to

$$s_b = s_m (1-z_m/f_m) , \qquad (110)$$

where s_m is the radius of the beam on the mirror, f_m is the focal length of the mirror, and s_b is the beam radius at a distance z_m from the mirror. Then, as it leaves this last mirror, the beam waist will also converge at the same rate as the restricted beam. Therefore, the spot size or beam waist at some distance z_m from the focusing mirror is

$$w_{z_m} = w_m (1 - z_m/f_m) , \qquad (111)$$

where w_m is the beam waist at the mirror obtained from Equation (108).

8.4.c. Laser Power and Electric Field Amplitude

To determine the electric field amplitude (ε_ℓ) of the laser, the laser power (P) is measured at some distance z_m from the focusing mirror. The quantities P and ε_ℓ are related by

$$P_\ell = \frac{\varepsilon_\ell^2 cA}{8\pi} \tag{112}$$

where c is the speed of light and A is the cross-sectional area of the beam. In this equation P and ε_ℓ^2 are average values.

In conclusion, the average power is measured from which the average electric field amplitude can be calculated, since the cross-sectional area of the beam can be determined once the limiting spot size has been calculated.

8.5. Transition Dipole Moments

The transition dipole moments (μ_{fi}) are determined as follows,[82]

$$\mu_{fi} = \int \Psi_f^* \mu_y \Psi_i dQd\underset{\sim}{\theta} \tag{113}$$

where the integration is over the normal coordinate space Q and the rotational space $\underset{\sim}{\theta}$. The y component of the dipole moment is needed here because the direction of the Stark

field has been chosen to be the z direction and the laser electric field is polarized perpendicular to the Stark field. The total wave function (Ψ) for each state is the product of a rotational and a vibrational wave function,

$$\Psi_j = \psi_j^V \psi_j^R \quad . \tag{114}$$

The initial state vibrational wave function (ψ_i^V) is

$$\psi_i^V = \prod_m \phi_{v_m}(Q_m) \quad , \tag{115}$$

where $v_m = 0$ for all m in the transition studied here. Similarly, for the final state vibrational wave function,

$$\psi_f = \prod_n \phi_{v_n}(Q_n) \quad , \tag{116}$$

where $v_n = 0$ for all n except $v_3 = 1$. The rotational wave functions are

$$\psi_i^R = \psi^R(J''K''M'') \tag{117}$$

and

$$\psi_f^R = \psi^R(J'K'M') \quad . \tag{118}$$

The molecular dipole moment (μ_y) is

$$\mu_y = \mu_a \cos\theta_{ya} + \mu_b \cos\theta_{yb} + \mu_c \cos\theta_{yc} \ , \tag{119}$$

or

$$\mu_y = \mu_y^a + \mu_y^b + \mu_y^c \ , \tag{120}$$

where the a, b and c refer to the principal molecular frame of reference coordinates and the x, y, and z the laboratory frame of reference coordinates; in both vector spaces the origin is at the center of mass. The dipole moments μ_a, μ_b, and μ_c may be expanded in a Maclaurin series of the normal coordinates (Q_k), as follows:

$$\mu_g = \mu_g^o + \sum_k \left(\frac{\partial\mu_g}{\partial Q_k}\right) \ . \tag{121}$$

Then, the transition dipole moment (μ_{fi}) is

$$\mu_{fi} = (\mu_y^a)_{fi} + (\mu_y^b)_{fi} + (\mu_y^c)_{fi} \ , \tag{122}$$

in which

$$(\mu_y^g)_{fi} = \int \prod_j \psi_{v_j}^*(Q_j) \psi^R(J'K'M') \left[\mu_g^o + \sum \left(\frac{\partial\mu_g}{\partial Q_k}\right)_o Q_k\right]\cos\theta_{yg}$$

$$\prod_\ell \psi_{v_\ell}(Q_\ell) \psi^R(J''K''M'')d\underset{\sim}{\theta}d\underset{\sim}{Q} \ . \tag{123}$$

Finally, Equation (123) reduces to

$$(\mu_y^g)_{fi} = \mu_g^o \int \psi^R(J'K'M') \cos\theta_{yg} \psi^R(J''K''M'') d\theta \, \delta_{\underset{\sim}{v}',\underset{\sim}{v}''} +$$

$$\sum_k (\frac{\partial\mu_g}{\partial Q_k})_o \int \psi_{v_i}^*(Q_i) Q_i \psi_o dQ_i \int \psi^R(J'K'M') \cos\theta_{yg} \psi^R(J''K''M'') d\theta.$$

$$(124)$$

For the R(4,3) transition in the ν_3 band of $^{13}CH_3F$, the vibrational integral multiplying μ_g^o vanishes for all g and the only non-zero $(\partial\mu_g/\partial Q_k)_o$ is $(\partial\mu_g/\partial Q_3)_o$. Therefore,

$$\mu_{fi} = (\frac{\partial\mu_g}{\partial Q_3}) \int \psi_{v_3=1} Q_e \psi_{v_3=0} d\underset{\sim}{Q} \int \psi^R(5,3,M\pm1) \cos\theta_{ya} \psi^R(4,3,M) d\theta$$

$$(125)$$

and[67]

$$\int \psi_{v_3=1} Q_3 \psi_{v_3=0} dQ = (\frac{1}{2\gamma_3})^{\frac{1}{2}},$$

$$(126)$$

in which

$$\gamma_3 = 4\pi^2 \nu_3/h.$$

$$(127)$$

Also,

$$(\frac{\partial\mu_a}{\partial Q_e})^2 = \frac{3c^2\nu_3\Gamma_3}{N\pi d_3},$$

$$(128)$$

where Γ_3 is the area of the absorption band for the transition of frequency ν_3 with degeneracy $d_3 = 1$. Also,[56]

$$\int \psi^R (J+1,k,M\pm 1) \cos\theta_{ya} \psi^R (J,k,M) =$$

$$\mp \frac{[(J+1)^2 - K^2]^{\frac{1}{2}} [(J\pm M+1)(J\pm M+2)]^{\frac{1}{2}}}{2(J+1)[(2J+1)(2J+3)]^{\frac{1}{2}}} \qquad (129)$$

8.6. Wall Broadening

from the previous section on laser power and beam divergence the dimensions of the beam inside the Stark cell can be determined. The geometry of the beam in the cell then is a frustum of a right circular cone with the base of smaller radius at the far end of the Stark plates and the altitude equal to the length of the Stark plates. The wall broadening relaxation parameter can be determined by[62]

$$\Delta\omega_{w.b.} = \frac{A}{V} \left(\frac{RT}{8\pi^3 M}\right)^{\frac{1}{2}} , \qquad (130)$$

where T is the absolute temperature, M is the molecular mass of the sample, and R is the gas constant. The total surface area of the frustum (A) is[83]

$$A = \pi\{R_1^2 + R_2^2 + (R_1+R_2)[(R_1-R_2)^2 + h^2]^{\frac{1}{2}}\} , \qquad (131)$$

and the corresponding volume (V) is[68]

$$V = \frac{1}{3}\pi h (R_1^2 + R_2^2 + R_1 R_2) \quad , \tag{132}$$

where h is the altitude, R_1 is the radius of the larger base, and R_2 is the radius of the smaller base.

CHAPTER IX

RESULTS AND CONCLUSIONS

9.1. Stabilization Test Results

In all of the previous CO_2/N_2O laser experiments performed in our laboratory, the laser was stabilized by a dither technique. The piezoelectric translator (PZT), which supports the partially transmitting mirror, is forced to oscillate at 520 Hz by superimposing a sine wave voltage on the high DC voltage that is used to expand or contract the translator. The laser output power is detected and processed by a lock in amplifier which provides a feedback signal to the PZT. The signal adjusts the cavity length to keep the laser frequency at the top of the laser gain profile. In the present experiments a new stabilization technique (at least to our laboratory) was used. The laser was locked to the minimum in the saturation dip in the fluorescence from CO_2 in a sample cell in the laser cavity.[84-86] A comparison of the quality of the two methods will be discussed here.

Both laser stabilization methods were used to measure the laser Stark Lamp dip of a CH_3F Q(1,1) $-1\leftarrow0$ transition. In both cases several measurements were made in a single

day, as well as from day to day. The data were collected
on the PDP8/E computer with the BOXM program and the LDFIT
program was used to fit the line shapes. What was of in-
terest in these experiments was the reproducibility of the
center frequency or center Stark electric field, of the
selected transition. Also, free running laser data were
taken for comparison.

In the fluorescence stabilization method the center
Stark voltage of 1325.95 volts has a standard error in the
fit of 0.09 volts within a day and 0.19 volts from day to
day, while the dither stabilization method has a standard
error in the center voltage (1322.59 volts) of 0.91 volts
within a day. The free running laser Lamb dip data has a
standard error in the center voltage of 1.02 volts within a
day and 2.16 volts standard error in the data from day to
day.

Figures 7, 8, and 9 are oscilloscope pictures of the
Q(1,1) $-1 \leftarrow 0$ transition, one for each of the stabilization
methods. It was noted in the course of analyzing the data
that the dither stabilization also locks the laser to a
center voltage ~ 3.4 volts lower in field than the fluores-
cence technique. In conclusion, the laser Stark center
voltage is reproducible to a center position with ten
times greater accuracy when the fluorescent stabilization
is used rather than the dither method; also, the signal to
noise is better (see Figures 7, 8, and 9).

Figure 7.   A photograph of an oscilloscope plot of a
data file for the Q(1,1) m = -1←0 Lamb dip
transition in methyl fluoride under the ex-
perimental conditions of fluorescence stabiliza-
tion.

Figure 8.   A photograph of an oscilloscope trace of a Lamb
dip data file for the Q(1,1) m = -1←0 transition
in methyl fluoride under the experimental con-
dition where the laser was locked on top of
the laser gain profile.

Figure 9.   A photograph of an oscilloscope trace of a Lamb
dip data file for the Q(1,1) m = -1←0 transition
in methyl fluoride under the experimental condi-
tions of a free running laser (unlocked).
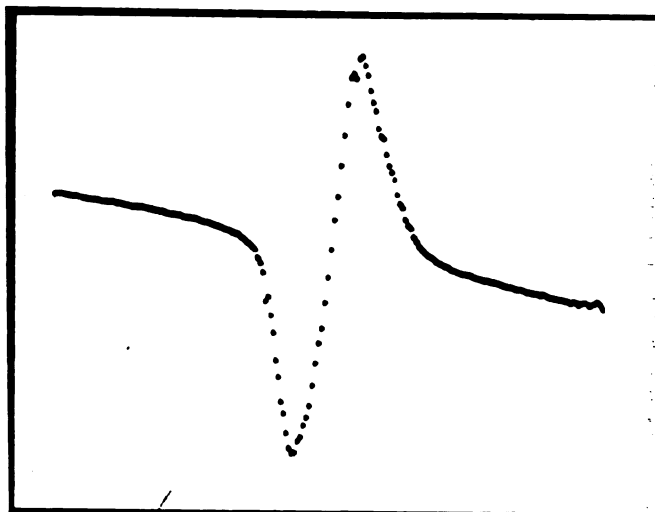
Figure 7
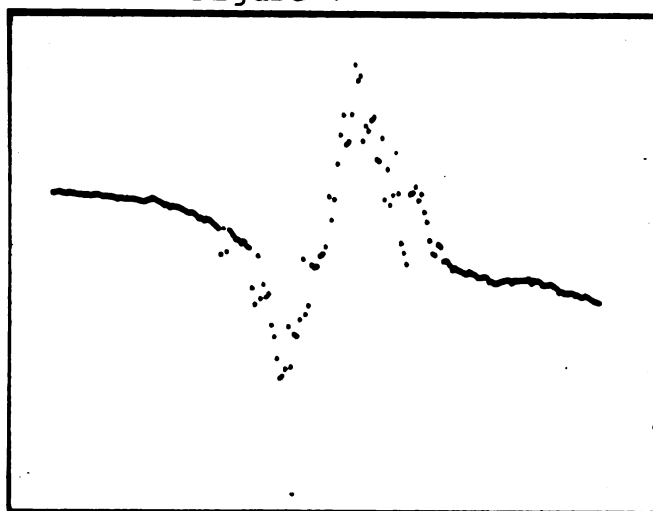
Figure 8

Figure 9

9.2. Modulation Broadening

When small amplitude modulation techniques are used where the experimental information is dependent on the line shape, it is very important that the modulation does not distort the line shape. In order to determine whether modulation broadening is contributing to the line shape in the present experiments, some computer experiments were performed in which theoretical modulation-broadened line shapes were generated and fit. The modulation amplitudes and the parameters used in the calculated line shapes were comparable to those obtained for the experimental data.

The computer program used to generate the modulation broadened data is a PDP-8 program called MODLVX, an abbreviation for modulation broadened level crossing. A comparison of these results of the theoretically generated data with that of the fits of experimental data taken under conditions of comparable pressure broadening is represented in Figure 10. In this figure, the derived value of the pressure broadening parameter is plotted against the modulation amplitude in volts. It should be noted that the modulation broadening for the highest modulation amplitude is still less than the scatter in the experimental data. Also, the total length of the ordinate shown is only ∿8% of the modulation broadened value of the half width. It was concluded that modulation broadening is not a significant contribution to the half width in these experiments.

Figure 10. A graphical representation of the effects of modulation broadening on the pressure broadening parameter.

EFFECT OF MODULATION BROADENING

Experimental Conditions

Pressure of 24.97 ± 0.25 millitorr
Temperture of 296.5 ± 0.1 K

$\Delta\nu_L$ (volts/cm)

PEAK MODULATION AMPLITUDE   (volts)
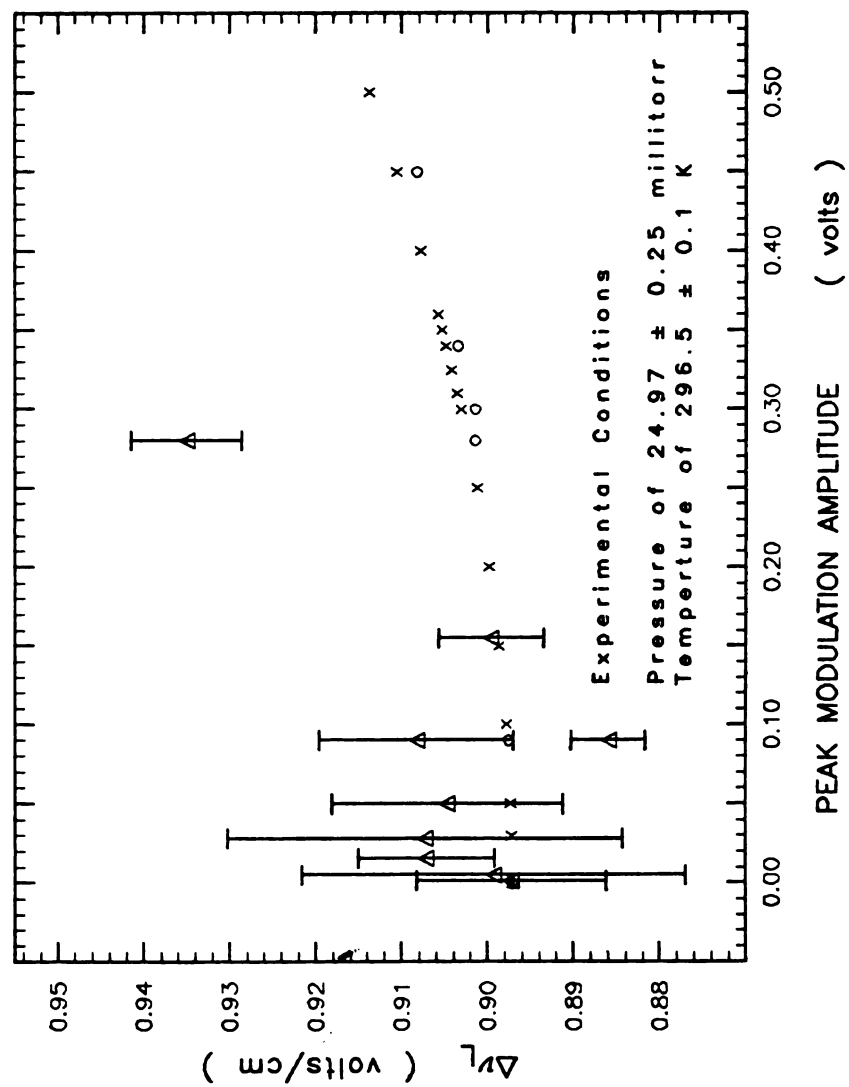
Figure 10

9.3. The Calculation of the Transition Dipole Moment

A transition dipole moment must be calculated for each of the possible transitions in the $^{13}CH_3F$ zero field level crossing. Since they are all ν_3 vibrational mode transitions, they will all have the same vibrational contribution; only the values of the magnetic quantum number changes. The vibrational contribution to the transition dipole moment has been calculated by Equations (126-128) and the values of these parameters are listed in Table (III). The rotational contribution to the transition dipole moments for the R(4,3) M±1←M transition are obtained by putting J = 4 into Equation (129). The transition dipole moments relevant to this investigation are listed in Table (IV).

9.4. The Laser Electric Field Amplitude Within the Stark Cell

In order to calculate the laser electric field amplitude in the Stark cell, as explained in section 8.4, the values of some important parameters are needed. The distance between the partially transmitting mirror and the grating is ∿4.25 meters and the radius of curvature of the output mirror is 10 meters, this mirror is made of germanium which has an index of refraction of 4.0. The CO_2 laser is oscillating on the 9P(32) laser line, which has a wavelength of 9.657 μm.

Table III. The Vibrational Parameters for the Transition
Dipole Moment of the CH_3F ν_3 Band.

Parameter	Value
Γ_3	9055.6 cm^2/mole[a]
$\omega_3{}^c$	1067 cm^{-1} [b]
d_3	1
$\nu_3{}^c$	1048.6 cm^{-1} [b]
$\partial\mu/\partial Q_3$	$\pm$117 $cm^{3/2}$/sec
γ	1.633 x 10^{-21} $erg^{\frac{1}{2}} \cdot$sec

[a]J. W. Russell, C. D. Needham, J. Overend, J. Chem. Phys.
45, 3383-3398, (1966), Table IX. S. Kondo, S. Shinnosuke,
J. Chem. Phys. 76, 809-816 (1982).

[b]J. Aldous, I. M. Mills, Spectrochemica Acta 18, 1071-
1091 (1962), Table 4. S. A. Rackley, R. J. Butcher, M.
Römheld, S. M. Freund, T. Oka, J. Mol. Spec. 92, 203-217,
(1982).

[c]ν_3 is the observed fundamental vibrational frequency and
ω_3 is the corrected harmonic frequency (corrected for an-
harmonic effects).

Table IV. The Transition Dipole Moments for all the Dif-
ferent m State Changes in the R(4,3) Zero Field
Level Crossing Transitions of $^{13}CH_3F$.

Transition J'K'M' ← J"K"M"		$\mu_{fi}/(D)$
53-5	43-4	-0.0729
53-3	43-4	+0.0109
53-4	43-3	-0.0652
53-2	43-3	+0.0188
53-3	43-2	-0.0575
53-1	43-2	+0.0266
53-2	43-1	-0.0498
53 0	43-1	+0.0344
53-1	43 0	-0.0421
53 1	43 0	+0.0421
53 0	43 1	-0.0344
53 2	43 1	+0.0498
53 1	43 2	-0.0266
53 3	43 2	+0.0575
53 2	43 3	-0.0188
53 4	43 3	+0.0652
53 3	43 4	-0.0109
53 5	43 4	+0.0729

The beam waist calculated at the surface of the output mirror is $w_m = 0.514$ cm. The beam at any point a distance z from the surface of this mirror may be calculated by Equation (108) to be $w_z = 0.514 + z \, (1.08 \times 10^{-3})$ cm. This equation is valid until the laser beam is reflected off the 4 meter radius of curvature focusing mirror, a distance of 2.1 meters from the partially transmitting mirror. From the focusing mirror the laser beam waist size may be calculated from Equation (111) to be $w = 0.730 \, (1-z/200)$. Here, the parameter z is the distance from the focusing mirror not from the partially transmitting mirror.

From the equations just given, the beam waist is 0.292 cm in the center of the Stark cell, which is approximately 120 cm from the focusing mirror. The center of the Stark cell was chosen because this will represent an average for the laser electric field amplitude along the z axis. Then, all that is needed is the average of the electric field across the beam.

The beam is limited by two diaphragms, the second or last one being located 70 cm before the focusing mirror with a nominal opening of 0.3 cm in diameter. The laser beam is still diverging from this point at the same rate that it left the laser so that the actual beam on the focusing mirror has a 0.171 cm radius, and the actual radius of the beam in the center of the Stark cell is 0.0684 cm.

The last part of the calculations of the electric field in the Stark cell involves the conversion of the

laser power measurement to electric field. For this pur-
pose, the power measurements listed in Table (V) for each
day that line shapes were recorded and the estimated beam
radius in the center of the Stark cell can be used in
Equation (112) to calculate a laser electric field ampli-
tude. The value for the root mean square value of the laser
electric field are also listed in Table (V).

9.5. Wall Broadening and Power Broadening

Since the laser electric field amplitude and the tran-
sition dipole moments have just been calculated it would
be appropriate to mention something about the power broad-
ening. Wall broadening has been placed in this section
because both the power broadening and the wall broadening
contribute to the intercept in the plot of Lorentzian half
width as a function of pressure (Figure 11, which will be
discussed later). The laser power broadening factor is
the product of the laser electric field amplitude and the
transition dipole moment divided by Planck's constant, it
ranges from 0.772 MHz to 0.116 MHz for these experiments.

In the plot in Figure 11 the theoretical calculations
were generated with the most common experimental laser
electric field amplitude of 22.8 volts/cm. The theoretical
data have an intercept of 1.89±0.089 volts/cm (±2σ) and the
experimental linear least squares intercept is 2.09±0.096
volts/cm (±2σ).

Table V. Laser Power Measurement and Corresponding Cal-
culated Laser Electric Field Amplitude.

Date	$<P_\ell>_{In}$/[a] (mW)	$<P_\ell>_{Out}$/[b] (mW)	$<\varepsilon^2>^{1/2}$/[c] (Volts/cm)	$<\varepsilon^2>^{1/2}$/[d] (Volts/cm)
Oct. 2	17.5	1.0	30.0	15.9
Oct. 5	33.9	10.0	41.7	27.0
Oct. 6	21.6	8.0	33.2	22.8
Oct. 7	25.4	7.5	36.1	23.4
Oct. 8	29.1	11.0	38.6	26.6

[a] An average laser power before the Stark cell.

[b] An average laser power after the Stark cell.

[c] r.m.s. electric field amplitude in the center of the Stark cell, assuming no losses at the windows.

[d] r.m.s. electric field amplitude in the center of the Stark cell assuming half the laser loss in passing through the cell occurs at the first window.

Figure 11. Plot of the pressure broadening $\underline{vs}$. pressure
            for the R(4,3) zero field level crossing in the
            ν_3 band of $^{13}CH_3F$. The dotted line represents
            the linear least squares fit of the experimenta
            data and the dashed line the linear least
            squares fit of the theoretical data.

PRESSURE BROADENING OF $^{13}CH_3F$
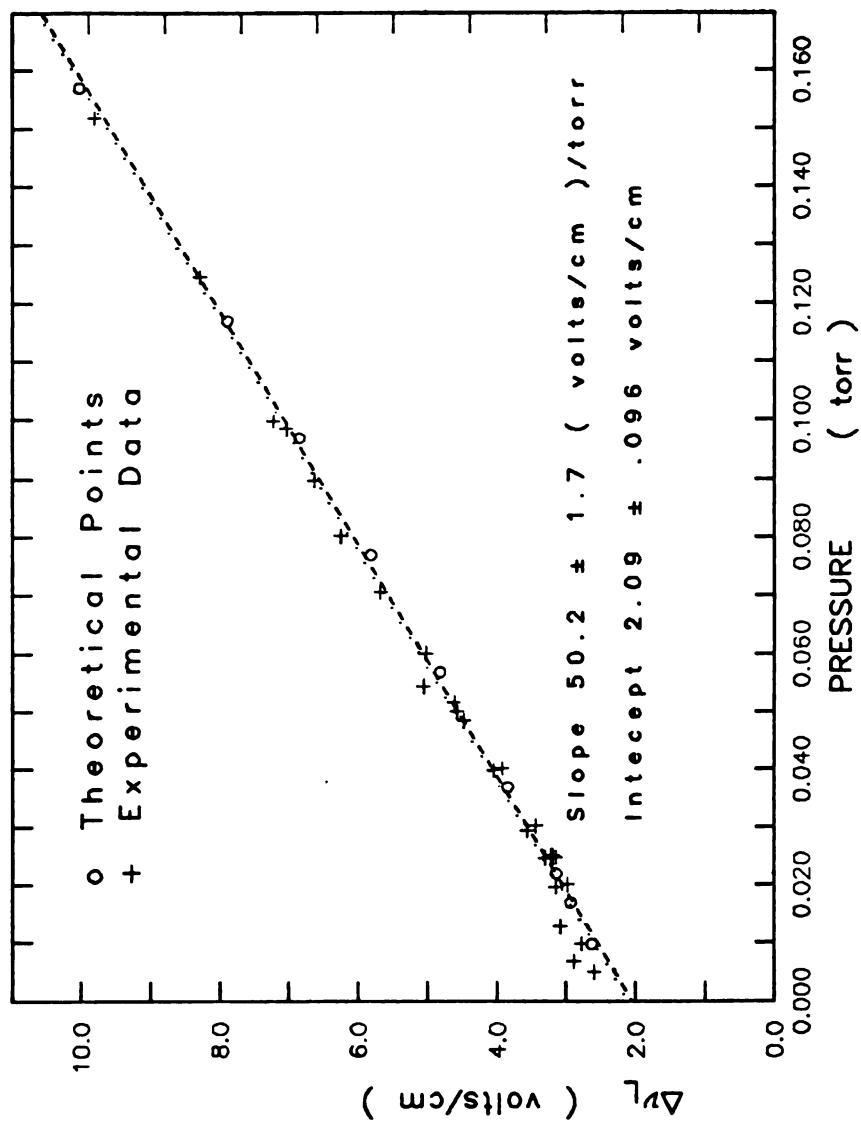
Figure 11

The wall broadening parameter calculated by the kinetic theory of gases and Equation (130) is 48 kHz, based on the assumption that the geometry of the laser beam can be represented by a frustum of a right circular cone. When the wall broadening effect has been accounted for in the pressure broadening of the profile a theoretical intercept of 2.04 ± 0.086 volts/cm ($\pm2\sigma$) is calculated which is 2.6% less than the experimental intercept.

9.6.a. Pressure Broadening: Experimental Data

The experimental data were recorded under various experimental conditions (modulation amplitude, Stark field sweep width, laser power, and temperature). The experimentally determined half widths at half maximum for the pressure broadening contribution to the line shape were corrected to common values for these various experimental parameters by the following equations,

$$\Delta\nu_L = \Delta\nu_{L_{Exp.}} + \left(\frac{\partial\Delta\nu_L}{\partial MA}\right) dMA + \left(\frac{\partial\Delta\nu_L}{\partial SW}\right) dSW + \left(\frac{\partial\Delta\nu_L}{\partial LF}\right) dLF +$$

$$+ \left(\frac{\partial\Delta\nu_L}{\partial T}\right) dT . \tag{133}$$

The partial derivative with respect to the modulation amplitude (MA) is determined from the MODLVX program output (see Section 9.2 on modulation broadening). All of the

experimental data were corrected to zero modulation am-
plitude. The partial derivative with respect to the Stark
field sweep width (SW) is determined from the theoretical
calculations intrinsic to the LVX2 program (Figure 12).
The LVX2 program was also used to generate information on
the partial derivative with respect to the laser electric
field amplitude (LF), Figure 13. The data were corrected
to the experimental value for which the most experimental
measurements were made in both the laser electric field
amplitude and Stark sweep width case. No temperature cor-
rections were deemed necessary, once it was determined
that the experimental temperature 296.36±0.36 K (±2σ) was
very stable, even from day to day.

A list of the corrected experimental data is given in
Table (VI). In this table the experimental pressure broad-
ened half widths are the average of five experimental data
files, two standard deviation error bars are reported. The
pressure broadened half widths reported in Table (VI) are
in volts/cm rather than in frequency units. This results
from the fact that the sixteen overlapping zero field level
crossing transitions have different Stark slopes (derivatives
of frequency with respect to the Stark electric field).
The line shape is a superposition of the sixteen transitions
and cannot be deconvoluted into its separate components.
Therefore, the transformation of the individual half widths
to frequency units cannot be performed.

Figure 12. A graphical representation of how the Stark
            field sweep width affects the determined pres-
            sure broadening parameter.

GRAPH OF THE LORENTZIAN HALF WIDTH AS
A FUNCTION OF THE STARK FIELD SWEEP
WIDTH

o Gaussian - Lorentzian
+ Polynomial - Lorentzian

STARK FIELD SWEEP WIDTH   (volts/cm)

$\Delta \nu_L$ (volts/cm)

Figure 12

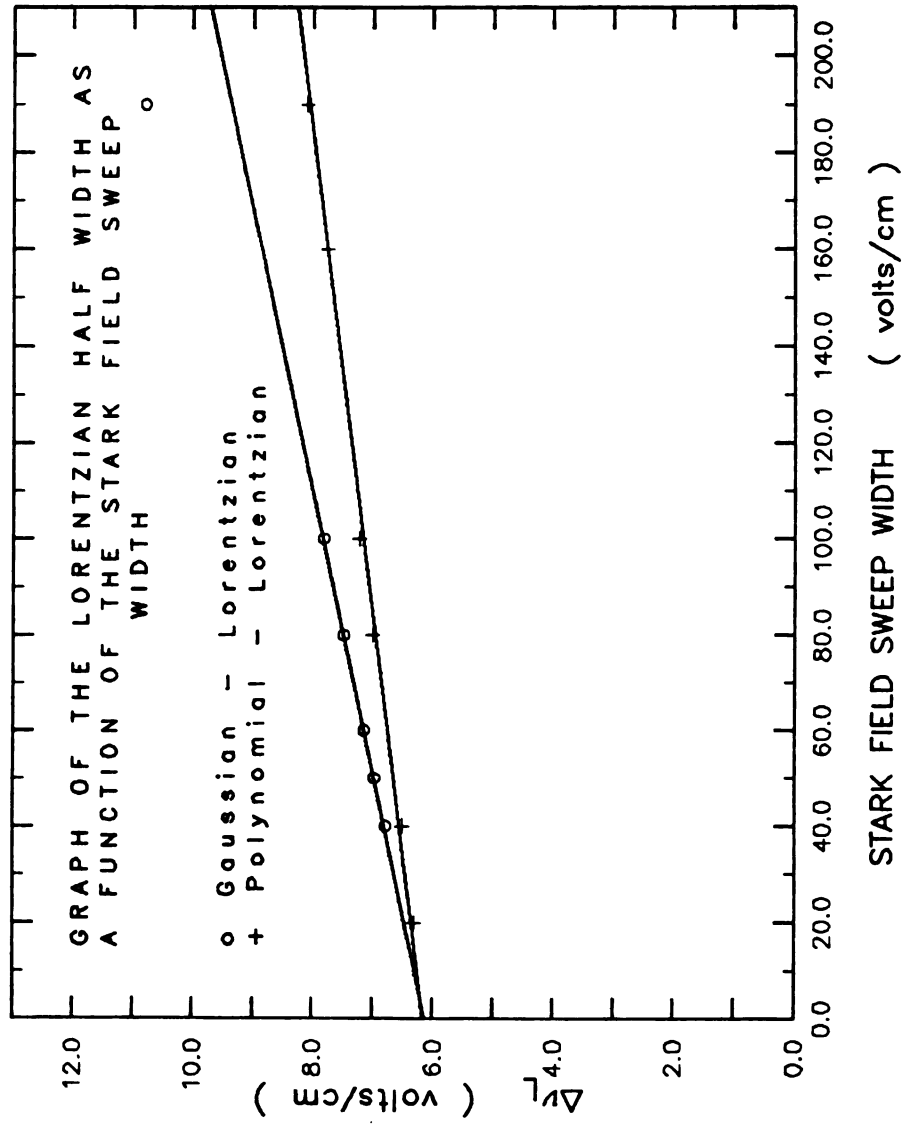Figure 13. A graphical representation of how the laser
            electric field amplitude power broadens the
            determined pressure broadening parameter.

GRAPH OF THE LORENTZIAN HALF WIDTH AS
A FUNCTION OF THE LASER ELECTRIC FIELD
AMPLITUDE

o Stark Field Sweep Width of 60 volts/cm
+ Stark Field Sweep Width of 80 volts/cm

LASER ELECTRIC FIELD AMPLITUDE (volts/cm)

$\Delta\nu_L$ (volts/cm)
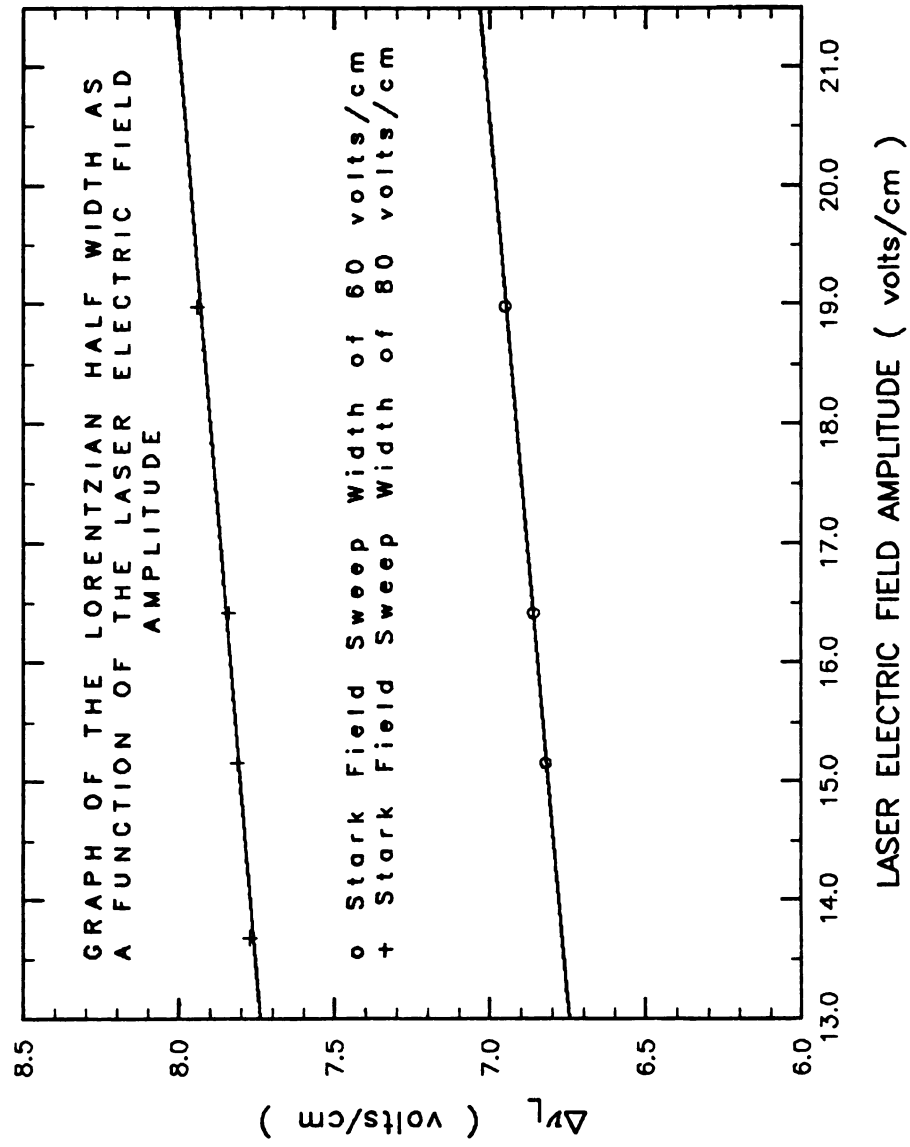
Figure 13

Table VI. Pressure Broadening Parameters as a Function of
Pressure for the Zero Field Level Crossing in the
$(J,K)=(5,3)\leftarrow(4,3)$ Transition in $^{13}CF_3F$.

| Experimental | | Theoretical | |
Pressure/ (millitorr)	$\Delta\nu_L/^{a,b}$ (Volts/cm)	Pressure/ (millitorr)	$\Delta\nu_L/^c$ (Volts/cm)
5.03	2.60±0.009	9.8	2.64±0.084
6.85	2.89±0.061	17.0	2.94±0.066
9.88	2.79±0.013	22.0	3.15±0.060
12.88	3.09±0.087	37.0	3.85±0.056
19.75	3.57±0.018	57.0	4.82±0.052
20.12	2.99±0.021	77.0	5.82±0.046
24.78	3.20±0.020	117.0	7.89±0.034
24.83	3.16±0.014	157.0	10.03±0.026
24.93	3.23±0.037		
24.96	3.22±0.044		
25.06	3.23±0.075		
25.11	3.23±0.026		
25.14	3.20±0.073		
25.18	3.20±0.036		
29.43	3.57±0.018		
30.21	3.44±0.046		
39.90	4.05±0.040		
40.25	3.93±0.023		
48.52	4.47±0.028		
50.09	4.57±0.053		
51.73	4.62±0.034		
54.57	5.06±0.026		
60.17	5.03±0.043		
70.72	5.68±0.074		
80.26	6.25±0.276		
89.82	6.63±0.064		
98.54	7.04±0.070		
99.87	7.23±0.152		
124.56	8.28±0.144		
151.81	9.81±0.536		

[a]Each experimental $\Delta\nu_L$ is the average of 5 values derived
from 5 experimental line shapes corrected for variations
in modulation amplitude, sweep width, and laser power.
The uncertainties are two standard deviations.

[b]$T=296.36\pm0.36$ K $(\pm2\sigma)$.

[c]The uncertainties are two standard errors.

9.6.b. Pressure Broadening: Theoretical Calculations

The theoretical data listed in Table VI were generated by means of the CYBER 750 program LVX2. For each calculation, a pressure broadening parameter, a sweep width, and a power broadening factor were assumed. The Stark field sweep width was set equal to the corrected value used in the experimental data. The power broadening factor was set equal to the value calculated by means of the expressions in the sections on laser electric field (8.4, 9.4) and transition dipole moment (8.5, 9.3).

The pressure broadening parameter was varied by extrapolation and interpolation until the slope of the theoretical data in Figure 11 matched that of the experimental data. It should be noted that the generated theoretical line shapes were not fit or generated as derivative line shapes, but rather as the more traditional line shapes.

9.7. Results and Conclusions

To obtain theoretical data co-linear with the experimental data (Figure 11) requires a pressure broadening parameter of 16.0±0.9 MHz/torr (±2σ). The slopes from the linear regression analysis of the theoretical and experimental data, 50.2±1.0 (volts/cm)/torr and 50.2±1.7 (volts/cm)/torr, respectively, were used to determine the error limits which are two standard errors. A comparison of

this result with the results from other methods and/or other transitions of CH_3F is shown in Table (VII). The experimental intercept is 2.09 ± 0.096 volts/cm and the theoretical intercept is 2.04 ± 0.086 volts/cm when both power broadening and beam transit effects are considered. The major contribution to the large intercept is the power broadening as noted in Section 9.5 and the major reason for the difference can then be traced back to the estimate of the laser electric field within the Stark cell.

Table VII. Comparison of Pressure Broadening Parameters for CH_3F.

Molecule	Transition JK→JK	Temp. (K)	Pressure Broadening Coefficient/ (MHz/torr)	Method
$^{13}CH_3F$ (90%)	5,3→4,3	296	16.0±0.9	Zero field level crossing[a]
$^{13}CH_3F$ (90%)	5,3→4,3	---	15.5	Optical nutation[b]
$^{13}CH_3F$ (62%)	4,3→3,3	---	15.2±0.8	Time resolved infrared[c]
	5,3→4,3	---	15.2±0.8	Microwave double resonance
CH_3F	1,0→0,0	300	20	Microwave line shape[d]
CH_3F	2,1→1,1	---	19	Transient Absorption[e]
CH_3F	1,0→0,0	---	20	Microwave echo[f]
CH_3F	3,0→2,0	300	17.2	Millimeter wave[g]
	3,1→2,1	300	17.2	Line shapes
	3,2→2,2	300	17.2±0.6	

[a] These experiments.

[b] Brewer, Shoemaker, Phys. Rev. Lett. 27, 631-634 (1971).

[c] H. Jetter, E. F. Pearson, C. L. Norris, J. C. McGurk, W. H. Flygare, J. Chem. Phys. 59, 1796-1804 (1973).

Table VII. Continued.

[d]Gilliam, Edwards, Gordy, Phys. Rev. 75, 1014 (1949).

[e]F. Rohart, J. P. Prault, B. Macke, 35th Symposium on Molecular Spectroscopy, Columbus, Ohio 1980.

[f]P. Glorieux, J. Legrand, B. Macke, Chem. Phys. Lett., 40, 287-291 (1976).

[g]G. Birnbaum, E. R. Cohen, J. R. Rusk, J. Chem. Phys., 49, 5150-5156 (1968).

CHAPTER X

FINAL COMMENTS

In this chapter the two types of experiments performed in this investigation are compared. The strong as well as the weak points of line shape studies by both laser Stark spectroscopy and level crossing spectroscopy will be pointed out. Then a possible experiment that would have as many strong points as both techniques with fewer weak points than either will be described.

The measurement of a single laser Stark line shape is a relatively easy experiment, but in most cases it can be quite difficult to acquire a set of line shapes at reasonably different sample pressures. This is due to the fact that at moderate to high Stark fields electrical discharges in the sample cell cause extreme difficulties. That same Stark field can be beneficial in removing the degeneracy of a level, allowing only one transition to be studied, except for the unfortunate situation where overlapping transitions are encountered. Laser Stark line shapes can, and in most cases are, studied at low enough laser power that power broadening or saturation of the transition is not a significant contribution to a profile. Unfortunately,

separation of the inhomogeneous contribution from the homogeneous broadening mechanisms in the line shapes can cause problems, and the ever present modulation, that may cause modulation broadening, must be considered.

In level crossing and avoided crossing, which are saturation phenomena, there is no Doppler contribution to the line shape that must be removed. But rather, the Doppler broadening is a major contributor to the background on which the desired signal is superimposed. Unfortunately, this background is not linear. Since there is no Doppler contribution to the recorded profile, the level crossing signal is usually narrower than a laser Stark line shape, allowing for a smaller sweep width and higher resolution. In zero field level crossing experiments, like the one of concern here, there is no problem with a Stark field breakdown, but rather the difficult problems of power broadening and overlapping transitions have to be taken into consideration. Proper handling, measuring, and accounting for the laser electric field amplitude are essential. A major drawback for level crossing and especially zero field level crossing experiments is that they are rare. Transitions whose resonant frequencies are coincident with laser lines are not as common as laser Stark transitions. Again, as in the laser Stark line shape experiment, modulation broadening can be a serious problem.

A more ideal experiment then would be one in which all

of the strong points of both methods, with none of the weak points of either (except for the ubiquitous modulation broadening), are present. In an infrared microwave two-photon experiment the absence of a Stark field eliminates the problem of electrical breakdown, which can occur in laser Stark experiments, without the loss of tunability. The two-photon signal would have to be deconvoluted into its homogeneous and inhomogeneous components, but this is more easily performed than the combined background fitting and laser power estimation required for a level crossing experiment, and there would be no need for a transition that is coincident with the laser line. Preliminary experiments could be performed in which the laser and microwave powers are varied to determine appropriate radiation fields that would cause a minimal amount of power broadening.

REFERENCES

REFERENCES

1. M. A. Gordon, L. E. Snyder, <u>Molecules in the Galatic Environment</u>, John Wiley & Sons, New York (1973).

2. L. D. Tubbs, D. Williams, J. Opt. Soc. Am. <u>62</u>, 284-289 (1972).

3. T. Owen, H. P. Mason, AP. J. <u>154</u>, 317-326 (1968).

4. J. S. Margolis, J. Quant. Spectrosc. Radiat. Transfer. <u>11</u>, 69-73 (1971).

5. P. Varanasi, J. Quant. Spectrosc. Radiat. Transfer <u>11</u>, 1711-1724 (1971).

6. T. Kostiuk, M. J. Mumma, J. J. Hillman, D. Buhl, L. W. Brown, J. L. Faris, D. L. Spears, Infrared Phys. <u>17</u>, 431-439 (1977).

7. F. W. Taylor, J. Quant. Spectrosc. Radiat. Transfer <u>13</u>, 1181-1217 (1973).

8. P. Palmer, B. Zuckerman, D. Buhl, L. E. Snyder, AP. J. <u>156</u>, L147-L150 (1969).

9. C. Heiles, AP. J., <u>157</u>, 123-134 (1969).

10. C. Heiles, AP. J., <u>151</u>, 919-934 (1968).

11. P. Solomon, K. B. Jefferts, A. A. Penzias, R. W. Wilson AP.J., L53-L56 (1971).

12. W. H. Flygare, <u>Molecular Structure and Dynamics</u>, Prentice-Hall, Inc., NJ (1978).

13. F. J. Lovas, D. R. Johnson, D. Buhl, L. E. Snyder, AP. J. <u>209</u>, 770-777 (1976).

14. P. M. Solomon, D. B. Jefferts, A. A. Benzia, R. W. Wilson, AP.J. <u>168</u>, L107-L110 (1971).

15. J. Schmidt, P. R. Berman, R. G. Brewer, Phys. Rev. Letts, <u>31</u>, 1103-1106 (1973.

16. A. Schenzle, R. G. Brewer, Phys. Rev. A, <u>14</u>, 1756-1765 (1976).

17. R. G. Brewer, Sci., <u>178</u>, 247-255 (1972).

18. S. B. Grossman, A. Schenzle, R. G. Brewer, Phys. Rev. Letts. <u>38</u>, 275-278 (1977).

19. K. L. Foster, S. Stenholm, R. G. Brewer, Phys. Rev. A, <u>10</u>, 2318-2324 (1974).

20. P. B. Davis, H. Jones, Appl. Phys., <u>22</u>, 53-55 (1980).

21. W. A. Peeldes, D. L. Brower, N. C. Luhmann, Jr., E. J. Danielwicz, I.E.E.E., J. Quant. Elect., <u>QE-16</u>, 505-507 (1980).

22. T. Y. Chang, J. D. McGee, Appl. Phys. Lett., <u>19</u>, 103-105 (1971).

23. H. E. Radford, I.E.E.E. J. Quant. Elect., <u>QE-11</u>, 213-214 (1975).

24. Laser Focus, May, 44-46 (1981).

25. P. R. Berman, W. E. Lamb, Jr., Phys. Rev. A, <u>2</u>, 2435-2454 (1970).

26. M. Borenstein, W. E. Lamb, Jr., Phys. Rev. A. <u>5</u>, 1311-1323 (1972).

27. G. D. T. Tejwani, J. Chem. Phys. <u>57</u>, 4676-4681 (1972).

28. G. D. T. Tejwani, P. Varanasi, J. Quant. Spectrosc. Radiat. Transfer, <u>11</u>, 1659-1664 (1971).

29. S. A. Rackley, R. J. Butcher, M. Römheld, S. M. Freund, T. Oka, J. Mol. Spec., <u>92</u>, 203-217 (1982).

30. E. Bjarnov, R. H. Schwendeman, to be published.

31. M. Römheld, Dissertation, ULM (1978).

32. W. K. Voigt, Bayer. Akad München, Ber. 603 (1912).

33. E. Bjarnov, S. Sandholm, R. H. Schwendeman, 34th Symposium on Molecular Spectroscopy, WA10 (1979).

34. R. H. Dicke, Phys. Rev. <u>89</u>, 472-473 (1953).

35. A. S. Pine, J. Mol. Spec., <u>82</u>, 435-448 (1980).

36. D. R. Roa, T. Oka, 34th Symposium on Molecular Spectroscopy, RA4 (1979).

37. M. A. Henesian, L. Kulevskii, R. L. Byer, R. L. Herbst, Opt. Comm., 18, 225-226 (1976).

38. B. B. Krynetsky, L. A. Kulevsky, V. A. Mishin, A. M. Prokhorv, A. D. Savelev, V. V. Smirnov, Opt. Comm. 21, 225-228 (1977).

39. P. Lallemand, P. Simova, G. Bret, Phys. Rev. Letts. 17, 1239-1241 (1966).

40. J. R. Murray, A. Javan, J. Mol. Spec., 42, 1-26 (1972).

41. B. K. Gupta, S. Hess, A. D. May, Canad. J. Phys. 50, 778-782 (1972).

42. B. K. Gupta, A. D. May, Canad. J. Phys., 50, 1747-1755, (1972).

43. U. Fink, T. A. Wiggins, D. H. Rank, J. Mol. Spec., 18, 384-395 (1965).

44. J. Reed, A. R. W. McKellar, Phys. Rev. A18, 224-228 (1978).

45. A. R. W. McKellar, T. Oka, Canad. J. Phys. 56, 1315-1320 (1978).

46. H. L. Buijs, H. P. Gush, Canad. J. Phys., 49, 2366-2375 (1971).

47. R. S. Eng. A. R. Calaway, T. C. Harman, P. O. Kelley, A. Javan, Appl. Phys. Letts., 21, 303-305 (1972).

48. T. Amano, R. H. Schwendeman, J. Chem. Phys., 68, 530-537 (1978).

49. S. M. Freund, G. Duxbury, M. Römheld, J. T. Tiedje, T. Oka, J. Mol. Spec., 52, 38-57 (1974).

50. Walter Cleland, private communication.

51. J. A. Riddick, W. B. Bunger, Organic Solvents, Wiley Interscience, Vol. 2, p. 798-805 (1970).

52. S. Sandholm, Thesis, Michigan State University (1979).

53. S. G. Rautian, I. I. Sobel'mann, Soviet Phys. Uspeki, 9, 701-716 (1967).

54. J. I. Steinfeld, Molecules and Radiation, Harper & Row, New York, Chapter 12 (1974).

55. R. H. Schwendeman, unpublished.

56. M. W. P. Strandberg, Microwave Spectroscopy, John Wiley & Sons, Inc., New York, Chapter 1 (1954).

57. J. W. Strutt (Lord Rayleigh), Philos. Mag. 27, 298 (1889).

58. E. Fermi, Rev. Modern Physics, 4, 105-132 (1932).

59. L. Galatry, Phys. Rev. 122, 1218-1223 (1961).

60. M. Nelkin, A. Ghatak, Phys. Rev. A 135, 4-9 (1964).

61. J. I. Gersten, H. M. Foley, J. Opt. Soc. Amer. 58, 933-935 (1968).

62. C. H. Townes, A. L. Schawlow, Microwave Spectroscopy, Interscience Pub., New York, Section 15-16, p. 374 (1970).

63. J. D. Lambert, G. A. H. Roberts, J. S. Rowlinson, V. J. Wilkinson, Proc. Roy. Soc. London 196A, 113-125 (1949).

64. W. Hanle, Z. Phys. 30, 93-105 (1924).

65. F. D. Colegrove, P. A. Franken, R. R. Lewis, and R. H. Sands, Phys. Rev. Lett., 3, 420-422 (1959).

66. J. S. Leven, P. A. Bonczyk, and A. Javan, Phys. Rev. Lett., 22, 267-270 (1969).

67. J. van der Linde and F. W. Dalby, Canad. J. of Phy. 50, 287-297 (1972).

68. A. C. Luntz, R. G. Brewer, K. L. Foster, and J. D. Swallen, Phys. Rev. Lett., 23, 951-954 (1969).

69. A. C. Luntz, R. G. Brewer, J. Chem. Phys., 53, 3380-3381 (1970).

70. A. C. Luntz, Chem. Phys. Lett., 11, 186-187 (1971).

71. A. C. Luntz, J. D. Swallen, and R. G. Brewer, Chem. Phys. Lett., 14, 512-513 (1972).

72. P. Glorieux, J. Legrand, B. Macke, and B. Segard, Phys. Lett. A48, 187-188 (1974).

73. J. Sakai, and M. Katayama, Chem. Phys. Lett. 35, 395-398 (1975).

74. J. Sakai and M. Katayama, Appl. Phys. Lett., 28, 119-121, (1976).

75. H. Wieder and T. G. Eck, Phys. Rev., 153, 103-112 (1967).

76. T. Amano, R. H. Schwendeman, J. Mol. Spec., 78, 437-451 (1979).

77. I. Ozier and W. L. Meerts, Phys. Rev. Letts., 40, 226-229 (1978).

78. D. H. Levy, J. Chem. Phys., 56, 5493-5499 (1972).

79. K. Shimoda, Japan, J. Appl. Phys., 11, 564-571 (1972).

80. A. K. Levine, LASERS, Marcel Dekker, Inc., NY (1966) Chapter 5.

81. H. Kogelnik, T. Li, Proceedings of the IEEE, 54, 1312-1334 (1966).

82. E. B. Wilson, J. C. Decius, P. C. Cross, Molecular Vibrations, McGraw-Hill Co., NY (1955).

83. Standard Mathematical Tables 20ed., Chemical Rubber Co., Cleveland, OH, p. 17 (1972).

84. M. Ouhayoun, C. J. Bordé, Metrologia, 13, 149-150 (1977).

85. C. Freed, R. G. O'Donnell, Metrologia, 13, 151-156 (1977).

86. J. E. Thomas, M. J. Kelley, J.-P. Monchalin, N. A. Kurnit, A. Jovan, Rev. Sci. Instrum., 51, 240-243 (1980).